Marília Braga

SPECTRAL MODELING AND EVALUATION OF INSTANTANEOUS AND LONG-TERM SPECTRAL IMPACTS ON THE PERFORMANCE OF mc-Si AND NEW GENERATION CdTe PHOTOVOLTAICS IN WARM AND SUNNY CLIMATES

Qualificação para passagem direta ao doutorado submetida ao Programa de Pós-Graduação em Engenharia Civil da Universidade Federal de Santa Catarina para a obtenção do Grau de Doutor em Engenharia Civil
Orientador: Prof. Ricardo Rüther, Ph.D.

Florianópolis
2019

Marília Braga

SPECTRAL MODELING AND EVALUATION OF INSTANTANEOUS AND LONG-TERM SPECTRAL IMPACTS ON THE PERFORMANCE OF mc-Si AND NEW GENERATION CdTe PHOTOVOLTAICS IN WARM AND SUNNY CLIMATES

Esta proposta de projeto foi julgada adequada para a passagem direta ao doutorado pelo Programa de Pós-Graduação em Engenharia Civil da Universidade Federal de Santa Catarina

Florianópolis, xx de julho de 2019.

_____

Prof. Poliana Dias de Moraes, Dr.
Coordenadora do Curso

_____

Prof. Ricardo Rüther, Ph.D.
Orientador
Universidade Federal de Santa Catarina

Banca Examinadora:

_____

Prof. Arno Krenzinger, Dr.
Universidade Federal do Rio Grande do Sul

_____

Prof. Lawrence L. Kazmerski, Ph.D.
University of Colorado

_____

Prof. Roberto Lamberts, Ph.D.
Universidade Federal de Santa Catarina

_____

Prof. Saulo Güths, Dr.
Universidade Federal de Santa Catarina

“Keep your face to the sun and you will never see
the shadows.”
- Helen Keller

ABSTRACT

This doctoral thesis will present an analysis of spectral impacts on mc-Si and new generation CdTe in distinct regions of Brazil: Florianópolis-SC (27°S, 48°W) in the South, Assu-RN (5°S, 37°W) in the Northeast, and other locations to be determined based on availability of funding for purchasing and installing adequate equipment. As utility-scale PV power plants are progressively being deployed in the Brazilian Northeast, the need for evaluation of the spectral effects of local blue-biased spectra on the energy yield of different PV technologies arises, as well as the need for spectral correction of field peak-power measurements done during commissioning and system performance tests. Considering the high cost of adequate spectral measurement equipment, this thesis will also examine three previously proposed methods (Sandia's AM-only, Pwat and 2-parameter), and a new approach for the estimation of spectral impacts without the need for in loco measurements. The proposed methodology consists of the use of satellite data acquired from NASA's Giovanni platform as inputs for SMARTS 2.9.5 spectra model. Preliminary results for measured spectra showed that, for both locations, CdTe has significant spectral gains: up to 10% for Assu-RN (Northeastern Brazil) and 2% for Florianópolis-SC (Southern Brazil). A seasonal variation could also be detected for both sites, with lower spectral gains for CdTe - and higher for mc-Si - close to the Southern Hemisphere's winter solstice, due to higher air mass values and lower precipitable water content of the atmosphere. Out of the direct methods evaluated for mc-Si, Sandia's AM-only had the best results with a Mean Absolute Error (MAE) of 0.026, while the 2-parameter method resulted in a 0.032 MAE. For CdTe, 2-parameter method yielded the best results with a 0.011 MAE, while Pwat presented a MAE of 0.024. This doctoral thesis will also propose new coefficients based on local measurements for these direct methods, better fitted for the blue-biased spectrum found in warm and sunny Brazil. Preliminary results show that the proposed method using Giovanni data and SMARTS spectra modeling performed very well for mc-Si, yielding better results than the direct methods evaluated. For CdTe the proposed methodology did not perform as well as the direct methods evaluated. Initially, the proposed method was also applied to instantaneous measurements for three different times (and AM values) of the day for Florianópolis: 9:00, 12:00 and 15:00, yielding satisfactory results for IV curve spectral correction.

Keywords: PV performance; spectral response; spectral factor; spectral modeling; CdTe; SMARTS.

LIST OF ILLUSTRATIONS

Figure 1 - Development of the production of PV modules by technology (Fraunhofer Institute for Solar Energy Systems, 2019). 22
Figure 2 - Comparison of the efficiencies of the best PV cells produced in the laboratory x best PV module efficiencies for the year 2011 (Fraunhofer Institute for Solar Energy Systems, 2011). 23
Figure 3 - Comparison of the efficiencies of the best PV cells produced in the laboratory x best PV module efficiencies for the year 2018 (Fraunhofer Institute for Solar Energy Systems, 2019; Green et al., 2019). 23
Figure 4 - Extraterrestrial solar spectrum (blue line) along with ASTM G173-03 reference spectrum (red line). Absorption bands of ozone (O_3), water (H_2O) and carbon dioxide (CO_2) are indicated in the image. Ultraviolet (UV), visible (VIS) and infrared regions of the spectrum are also delineated (Dornelles et al., 2015). 25
Figure 5 - Individual impact of AM (a), AOD (b) and PW (c) on different PV technologies' performance ratio, using the SMARTS model (Rodrigo et al., 2017). 27
Figure 6 - Spectral response (SR) of the most wide-spread PV materials nowadays (Rodrigo et al., 2017). 30
Figure 7 - Quantum efficiency (QE) for different PV technologies (Minnaert and Veelaert, 2014). 30
Figure 8 - Classification of indexes for quantifying spectral influences in photovoltaic systems (Rodrigo et al., 2017). 32
Figure 9 - Solar measurement station located at the Fotovoltaica-UFSC research laboratory in Florianópolis-SC, Brazil (27°S, 48°W), numbered according to Table 2. 35
Figure 10 - On-site spectral measurements made with the EKO MS-720 portable spectroradiometer in Assu-RN, Brazil (5°S, 37°W).. 37
Figure 11 - Spectral responses for mc-Si (wider, red-shifted curve) and new generation CdTe (narrower, blue-shifted curve) used in the computation of spectral indexes in this thesis. 42
Figure 12 - Impact of the main environmental variables on the local spectrum: (a) air mass (AM); (b) precipitable water (PW); (c) aerosol optical depth @ 550nm (AOD_{550}); (d) ozone (O_3); and (e) carbon dioxide (CO_2). 49
Figure 13 - Impact of (a) AOD, (b) precipitable water and (c) air mass on the spectral factor for mc-Si (red squares) and new generation CdTe (blue diamonds). 51

Figure 14 - Environmental parameters for Florianópolis-SC, Brazil (27°S, 48°W) obtained from the Giovanni platform (NASA, n.d.). (a) precipitable water (b) AOD @ 550nm (c) O_3 and (d) CO_2. 52
Figure 15 - Comparison between the reference ASTM G173-03 spectrum (gray line, 52% BF) and spectra measured for Florianópolis-SC, Brazil (27°S, 48°W) on November 12th, 2017 at 12:00 (orange line, 55% BF) and for Assu-RN, Brazil (5°S, 37°W) on November 22nd, 2017 (yellow line, 57% BF). Spectra were normalized to match the reference spectrum irradiance over the measured wavelengths. 54
Figure 16 - Spectral factor for mc-Si (red squares) and new generation CdTe (blue diamonds) calculated for 15-minute-averaged spectral measurements during a clear day (Oct. 28th, 2017) in Florianópolis-SC, Brazil (27°S, 48°W) (a) and for several spectral measurements for clear days (Nov. through Dec. 2017) in Assu-RN, Brazil (5°S, 37°W) (b), along with air mass (gray Xs) and precipitable water values (yellow triangles)..... 56
Figure 17 - Comparison between modeled spectrum (SMARTS + Giovanni method) and measured spectrum for Florianópolis-SC, Brazil (27°S, 48°W) at three distinct times of a clear-day (Oct. 28th, 2017): 9:00 (a); 12:00 (b); and 15:00 (c). 58
Figure 18 - Measured global horizontal irradiance (orange line), corresponding optical air mass (gray Xs) and irradiance-weighted air mass (gray dashed line) and (a), and solar spectral distribution with 15-minute-averaged resolution (b) for a clear-day (Oct. 28th, 2017) in Florianópolis-SC, Brazil (27°S, 48°W). 60
Figure 19 - Comparison between modeled (Giovanni + SMARTS method with irradiance-filtered and weighted AM, orange curve) and measured irradiance-weighted daily spectrum (blue curve) for several diffuse fractions in Florianópolis-SC, Brazil (27°S, 48°W). 61
Figure 20 - Relative deviation between measured SF and SF computed from SMARTS modeled spectra using irradiance-filtered and weighted AM values for Florianópolis-SC, Brazil (27°S, 48°W) for mc-Si (red squares) and new generation CdTe (blue diamonds) as a function of diffuse fraction for the analyzed days. 62
Figure 21 - SF results for measured spectra (gray squares) in comparison with 2-parameter method (blue diamonds, mc-Si and CdTe), Sandia's AM method (orange triangles, mc-Si only) and precipitable water method (red triangles, CdTe only), for mc-Si (a) and new generation CdTe (b) in Florianópolis-SC, Brazil (27°S, 48°W). Daily irradiance-filtered and weighted air mass (gray Xs) and precipitable water (yellow triangles) are also displayed on both graphs. 64

Figure 22 - Correlation between direct methods and measured SF for mc-Si (a) and new generation CdTe (b) for a full year of data from Florianópolis-SC, Brazil (27°S, 48°W). Sandia's AM method is shown as orange triangles (mc-Si only), Pwat method as red triangles (CdTe only) and the 2-parameter method as blue diamonds (mc-Si and CdTe)..... 66
Figure 23 - Absolute deviation between SF calculated from measured spectra and SF estimated through Sandia's AM method (orange triangles, mc-Si only), Pwat method (red triangles, CdTe only), 2-parameter method (blue diamonds, mc-Si and CdTe) and the proposed Giovanni + SMARTS method (grays squares, mc-Si and CdTe) for mc-Si (a) and new generation CdTe (b) in Florianópolis-SC, Brazil (27°S, 48°W). 67
Figure 24 - Daily average air mass (gray Xs), precipitable water (yellow triangles) and spectral factor estimated from measured data for Assu-RN, Brazil (5°S, 37°W) using the 2-parameter (blue diamonds), AM-only (orange triangles) and Pwat-only (red triangles) methods, for mc-Si (a) and new-generation CdTe (b). 69

LIST OF TABLES

Table 1 - Characteristic atmospheric parameters for distinct Brazilian locations and ASTM G173-03.The standard deviation for the concentration values of ozone (O_3), precipitable water (PW), and AOD are shown in parentheses (Haag, 2012). 29
Table 2 - List of sensors installed at the Fotovoltaica-UFSC research laboratory in Florianópolis-SC, Brazil (27°S, 48°W), numbered according to Figure 9 36
Table 3 - Main specifications of the spectroradiometers used to obtain spectral data for the analysis. 37
Table 4 - Data sources within NASA Giovanni platform used in the present study. 39
Table 5 - Inputs for the SMARTS model used in the present study for Florianópolis-SC, Brazil (27°S, 48°W). 41
Table 6 - 2-parameter method coefficients for mc-Si and CdTe obtained from (Lee and Panchula, 2016). 45
Table 7 - Comparison between irradiance-weighted average SF and SF calculated from irradiance-weighted average spectrum for mc-Si and new generation CdTe for a clear day (Oct. 28th, 2017) in Florianópolis-SC, Brazil (27°S, 48°W). 59
Table 8 - Minimum and maximum daily irradiance-weighted and filtered averages, and annual irradiation-weighted averages for SF and measured environmental parameter for the Assu-RN, Brazil (5°S, 37°W) site. 70

LIST OF ABBREVIATIONS

AM	Air Mass
AOD	Aerosol Optical Depth
APE	Average Photon Energy
ASTM	American Society for Testing and Materials
a-Si	Amorphous Silicon
a-Si/µc-Si	Microcrystalline Silicon
BF	Blue Fraction
CdTe	Cadmium-Telluride
CIGS	Copper-Indium-Gallium-Selenide
c-Si	Crystalline Silicon
IR	Infrared
MM	Spectral Mismatch Factor
m-Si	Multi-crystalline Silicon
PV	Photovoltaics
PW	Precipitable Water
R&D	Research and Development
SF	Spectral Factor
SMARTS	Simple Model of the Atmospheric Radiative Transfer of Sunshine
STC	Standard Test Conditions
TOA	Top of Atmosphere
UV	Ultraviovel
VIS	Visible
WV	Water Wapor

TABLE OF CONTENTS

1 Introduction 17
1.1 Objectives 19
1.1.1 Objective 19
1.1.2 Specific scope of work to reach the objective 19
2 Literature Review 21
2.1 Photovoltaic Solar Energy 21
2.2 Photovoltaic Technologies 21
2.3 Solar Spectrum 24
2.3.1 Solar Radiation 24
2.3.2 Reference and Brazilian Spectral Distributions 28
2.3.3 Spectral Response 29
2.3.4 Spectral Indexes 31
3 Method 35
3.1 Measurement Setup 35
3.2 Satellite Data Acquisition 38
3.3 Solar Geometry Data 39
3.4 Spectra Modeling 39
3.5 Spectral Factor 40
3.6 SF Estimation 43
3.6.1 SMARTS + Giovanni Method 43
3.6.2 Direct Methods 44
4 Preliminary Results 47
4.1 Impact of Environmental Variables on the Local Spectrum . 47
4.2 Satellite Atmospheric Data 50
4.3 Spectral Impacts on mc-Si and CdTe in Two Distinct Regions of Brazil 53
4.4 Giovanni + SMARTS Method: Instantaneous Spectrum 57
4.5 Giovanni + SMARTS Method: Irradiance-Weighted Spectrum 59

4.6 Assessment of Direct Methods for SF Computation..... 63

5 Preliminary Conclusions 71

6 Workplan and Timeline..... 73

1 INTRODUCTION

Unforeseen and impressive photovoltaic (PV) module price reductions over the last 10 years (Kavlak et al., 2018) have led to massive falling prices - and rising capacity factors and performance ratios - of utility-scale PV power plants, especially in warm and sunny climates all over the world (Bolinger et al., 2015; Parkinson, 2017, 2016; Reich et al., 2012). Cheaper PV modules gave rise to a noticeable increase in inverter loading ratios (Burger and Rüther, 2006) in ground-mounted PV plants in recent years, adding more DC (PV) power to the same AC power converter (Bolinger et al., 2015; Deschamps and Rüther, 2019). Most of these large-scale PV projects aim at selling PV electricity under long-term contracts, and close to the $ 25/MWh mark or less. While the traditional silicon technologies (c-Si, both mono- and multi-crystalline) dominate the scene, with some 97% of the world market in 2018 (Mints, 2018), high-efficiency (18% in current production and prospects of 22% demonstrated efficiencies (Bosio et al., 2018; NREL, 2018) and large-area (2.5 m^2) new generation thin-film cadmium-telluride (CdTe) PV modules have recently been introduced in the market (First Solar, 2018a, 2018b; Strevel, 2017). These improved CdTe modules present some interesting features for utility-scale PV power plants in the same warm and sunny climates where record-low prices for solar electricity are being promised. While for mc-Si PV spectral effects do not play a significant role, the narrower spectral response of CdTe results in different behaviors depending on the spectral content of sunlight at a particular site (Tsuji et al., 2018). The lower temperature coefficient on power, and the blue-shifted spectral response when compared to mc-Si, render thin-film CdTe, and the no longer commercially-available amorphous silicon PV technologies, good performers in the warm, sunny, humid and bluer skies predominant in sunbelt regions of the world (Dash et al., 2017; Munshi et al., 2018; Nann and Emery, 1992; Rüther et al., 2002; Rüther and Livingstone, 1994).

After irradiance, temperature and soiling, the spectral content of sunlight is one of the predominant variables affecting the performance of PV devices in the field, and assessing spectral shifts from the standard ASTM G173-03 spectrum (ASTM, 2012) caused mainly by aerosols (quantified by the Aerosol Optical Depth – AOD parameter), precipitable water and air mass is a matter not only of scientific interest, but of economic importance as well. AOD increases due to haze and biomass burning have been found to have the greatest impact in the wavelength range from 400 to 500 nm (Perry and Troccoli, 2015), leading to a red-shift in the spectral irradiance. This shift affects negatively the blue-

biased spectral response of CdTe modules (Ye et al., 2014), especially new generation CdTe which shows a significant better response in the 350-500 nm wavelength range than earlier versions of this technology (First Solar, 2017).

Even though the effects of the spectral distribution of light on PV performance have been extensively studied, and there is clear evidence of their importance on energy predictions and data analysis of PV systems (Dirnberger et al., 2015a, 2015b; R Gottschalg et al., 2003; Huld and Gracia Amillo, 2015; King et al., 1997; Kinsey, 2015; Lee et al., 2015b; Nelson et al., 2013; Stark and Theristis, 2015), there is still very limited measured historical spectral data available (Huld et al., 2013), due to high costs of equipment, logistics and data collection and processing for continuous measurement of solar spectra (Myers and Gueymard, 2004).

Instantaneous spectrum measurement for field IV curve correction is also a concern, seen that it is required by international standards (International Electrotechnical Commission, 2009, 2008) and that local spectra might have great impact on peak power measurements (Lad et al., 2010; Nann and Emery, 1992; Roy et al., 2010). Even though portable spectroradiometers are commercially-available, instantaneous measurements of spectrum face nearly the same drawbacks as previously mentioned for routine measurements: expensive equipment, logistics for field measurements and time-consuming data processing.

Considering the difficulty of obtaining measured and historical spectral data, the importance of taking into consideration spectral effects on energy predictions of PV systems, and the need for spectral correction of field measurements, this work proposes a simplified methodology using satellite atmospheric data combined with instantaneous and average irradiance-weighted relative optical air mass to generate instantaneous and irradiance-weighted average spectral factors using the SMARTS 2.9.5 software. An evaluation of direct methods for the estimation of spectral factors for Brazil is also presented, including measured spectra, in order to validate the proposed method.

1.1 OBJECTIVES

1.1.1 Objective

This doctoral thesis project has the main goal of evaluating the spectral effects of the Brazilian climate on the two main commercially-available PV technologies at the moment: mc-Si and CdTe.

1.1.2 Specific scope of work to reach the objective

a) Perform spectral measurements and characterize the local spectrum, comparing it to the reference ASTM G-173 spectrum;
b) Verify the use of the SMARTS model along with satellite data for the approximation of spectra, comparing modeled and measured results;
c) Calculate and map spectral factors for key PV technologies for sites throughout the Brazilian territory;
d) Estimate spectral effects using previously proposed methods and a novel method using spectra modeling and satellite data, comparing it to measured results;
e) Fit previously proposed direct methods for spectral impact evaluation to the Brazilian climate and atmospheric conditions.

2 LITERATURE REVIEW

2.1 PHOTOVOLTAIC SOLAR ENERGY

The PV effect allows converting the power of sunlight directly into electrical power. This method of energy conversion presents great advantages, such as extreme simplicity, the absence of moving parts, modular characteristic (from mW to MW), short installation time, high reliability and low maintenance. In addition, the PV conversion is virtually silent, non-polluting and uses the sun as a renewable and virtually inexhaustible source of energy.

The PV conversion occurs using semiconductor materials, with silicon (Si) being the most used. In addition to silicon, thin-film cadmium-telluride (CdTe), Copper Indium Gallium Diselenide (CIGS), as well as other composite semiconductors are also used (Parida et al., 2011; Rüther, 2004).

2.2 PHOTOVOLTAIC TECHNOLOGIES

PV technologies can be divided into three categories or generations of PV modules. The first generation uses crystalline silicon (c-Si) cells, mono or multi-crystalline, with thickness in the 150-200 μm range, representing a more significant limitation in terms of cost reduction and production (Saga, 2010). The second generation also uses silicon, but in amorphous form (a-Si), besides other materials such as CdTe or CIGS. This generation has an emphasis on cost reduction using very thin layers (~ 1μm), hence also called thin films. The third generation was initially being defined as a technology that should have been abundant, non-toxic, thin-layer, extremely low production costs, and of intrinsically higher efficiency materials than single-junction devices, such as those presented in the first generation. This definition has been expanded to include other advanced PV technologies, such as organic PV cells (dye-cells) and perovskite cells. Although the third-generation of PV modules has a longer perspective of cost reduction in the long run, currently they still have costs compared to those from first and second generation, as well as low life expectancy and low efficiency when deposited in large areas (Green et al., 2016, 2015; Parida et al., 2011). Figure 1 illustrates the production development of PV modules by technology. It can be observed that the first generation technologies have the largest share of commercial production, with more than 95% of the market for the year 2017 (~ 62% multicrystalline and ~ 33% monocrystalline).

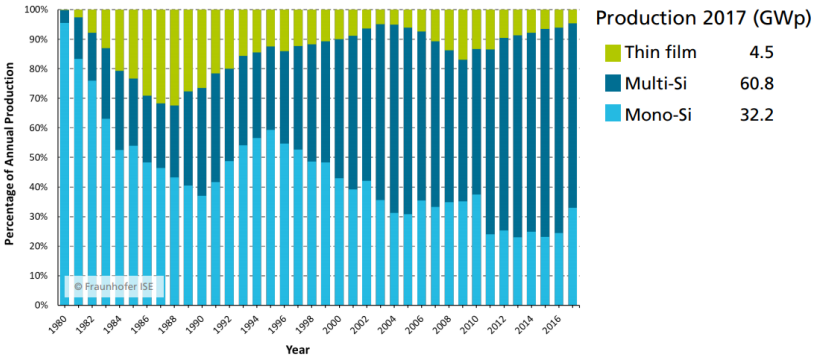


Figure 1 - Development of the production of PV modules by technology (Fraunhofer Institute for Solar Energy Systems, 2019).

The PV conversion efficiency is defined as the ratio of the maximum power produced by the cell or PV module, under standard test conditions (STC), to the product of the cell/module area and irradiance, also under STC (ABNT, 2006).

Figure 2 presents an efficiency comparison of the best PV cells produced in the laboratory and the best efficiencies of PV modules for the year 2011 and in Figure 3 for the year 2018. It is important to note that the presented efficiencies are much higher than those commercially available since laboratory studies generally use high purity materials in well-controlled production processes, as well as cells of reduced dimensions.

While the most widely used multi-crystalline silicon technology on the market had a 1.7% efficiency increase between 2011-2018 for the best modules, the best CdTe modules for the same period increased by 5.8%.

During the last 10 years, while the efficiency of commercially available and market-dominant multi-crystalline silicon modules increased from 12% to 17%, CdTe modules increased from 9% to 16% (Fraunhofer Institute for Solar Energy Systems, 2019).

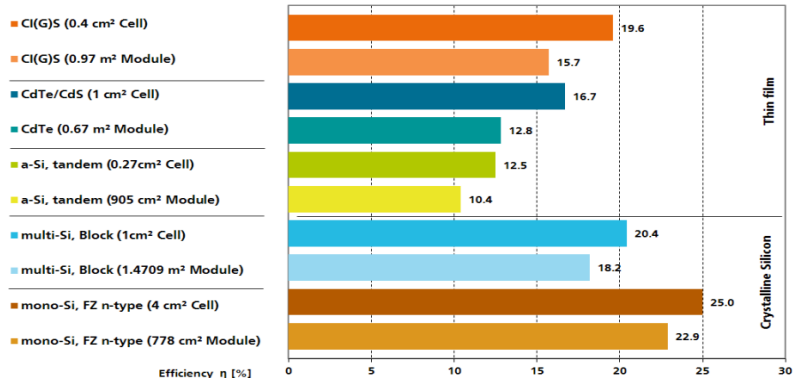


Figure 2 - Comparison of the efficiencies of the best PV cells produced in the laboratory x best PV module efficiencies for the year 2011 (Fraunhofer Institute for Solar Energy Systems, 2011).

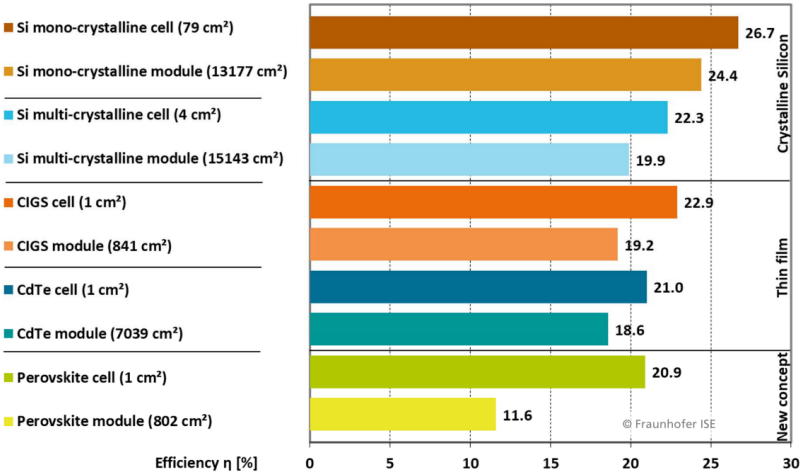


Figure 3 - Comparison of the efficiencies of the best PV cells produced in the laboratory x best PV module efficiencies for the year 2018 (Fraunhofer Institute for Solar Energy Systems, 2019; Green et al., 2019).

2.3 SOLAR SPECTRUM

2.3.1 Solar Radiation

The total radiation that reaches the Earth's top of atmosphere (TOA) can be calculated considering the Sun as a black body through the Stefan-Boltzmann's law ($E = \sigma T^4$). Considering an average radius of the Sun and the Sun-Earth distance, the total TOA radiance is approximately 1360 W/m^2, a value usually defined as the solar constant. The spectral distribution of light at the TOA is denominated extraterrestrial solar spectrum and can be found in Figure 4.

Figure 4 also presents the reference ASTM G173-03 spectrum (ASTM, 2012), proposed by the American Society for Testing and Materials (ASTM) in order to standardize PV device rating tests under standard test conditions (STC). Absorption bands of ozone (O_3), water (H_2O) and carbon dioxide (CO_2) are indicated in the image, as well as the ultraviolet (UV), visible (VIS) and infrared (IR) regions of the spectrum. The reference spectrum and how it compares to the local spectral distribution at the evaluated locations will be discussed later on.

After reaching the TOA, radiation must go through the Earth's atmosphere before reaching terrestrial semiconductor-based quantum converter devices, i.e. PV cells. In this trajectory, the atmosphere acts as a filter, modifying the amount and the spectral distribution of TOA solar radiation by scattering and absorption phenomena. The behavior of such filter (the atmosphere) depends on the amount of substance traversed by the solar rays in their course through the atmosphere and on the optical properties of the various atmospheric constituents (e.g. CH_4, O_2, CO_2, O_3, water vapor, aerosols, etc.). The Beer-Lambert law, shown in Eq. (1), describes the spectral distribution at the Earth's surface (E_λ) as a function of the extraterrestrial spectral distribution (E_{TR}), considering the optical depth of each i-extinction process for a given wavelength ($\tau_{i,\lambda}$) and optical air mass (m), which quantifies the amount of substance traversed by the sun rays with respect to a vertical trajectory.

$$E_\lambda = \mathrm{E_{TR}} \exp\left(-\sum_i m\tau_{i,\lambda}\right) \qquad \text{Eq. (1)}$$

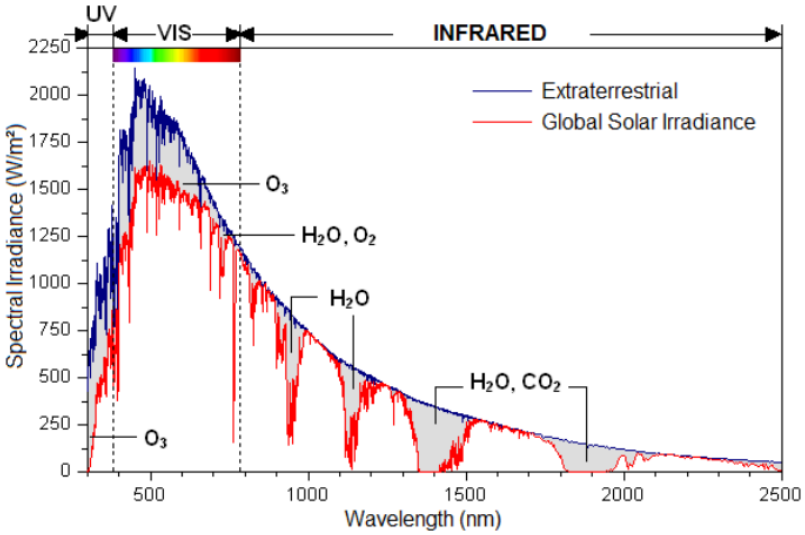


Figure 4 - Extraterrestrial solar spectrum (blue line) along with ASTM G173-03 reference spectrum (red line). Absorption bands of ozone (O_3), water (H_2O) and carbon dioxide (CO_2) are indicated in the image. Ultraviolet (UV), visible (VIS) and infrared regions of the spectrum are also delineated (Dornelles et al., 2015).

Even though each atmospheric constituent will have an optical air mass (AM) value, AM is usually reduced to a simple geometric parameter function of the solar position. The most widely used equation for AM as a function of the Sun's zenith angle (θ_z) was proposed by Gueymard (2003). The equation, which takes in consideration the Earth's spherical shape, is shown in Eq. (2). Increased AM values, usually found in high latitude regions and in the beginning and towards the end of the day in all regions, produce a significant attenuation on the ultraviolet (UV) region, red-shifting the spectral distribution.

$$AM = \cos\theta_z + \frac{0.4835\theta_z^{0.095846}}{96.7412 - \theta_z^{1.754}} \qquad \text{Eq. (2)}$$

Air mass, along with aerosol optical depth and water vapor are known to be the most relevant environmental parameters to affect spectral distribution of sunlight reaching the Earth's surface. These parameters are variable over space and time, and comments on each of them are made in the forthcoming paragraphs.

Suspended particles in the air in solid or liquid state that scatter and absorb radiation depending on its size and optical properties are called aerosols. The spectral attenuation of such particles is quantified by the aerosol optical depth (AOD). AOD can be estimated for a given wavelength (λ) by the Ångström turbidity equation, shown in Eq. (3), using the Ångström or wavelength exponent (α) and the aerosol optical depth, usually measured at 550 nm (AOD_{550}) (Eltbaakh et al., 2012). AOD has a greater impact on the spectral distribution on the UV-visible region of the spectrum, also resulting in a red shift of spectral distribution.

$$AOD = AOD_{550}\left(\frac{\lambda}{0.55}\right)^{-\alpha} \qquad \text{Eq. (3)}$$

Another important constituent of the Earth's atmosphere affecting terrestrial spectral distribution is water vapor. The most common approach to quantify water vapor in the atmosphere is using precipitable water (PW) that corresponds to the water column (usually in cm) that would be obtained if all water vapor overhead was to be condensed (Gueymard, 2014). An increase in precipitable water results in a strong attenuation on the near-infrared region of the spectrum, and therefore, a blue-shift of the spectral distribution.

The above-mentioned factors will produce different effects on the performance of photovoltaic devices depending on their absorption bands. These effects have been previously investigated using the SMARTS (Simple Model of the Atmospheric Radiative Transfer of Sunshine) model and reference spectrum parameters, changing one environmental variable at a time (Fernandez et al., 2015; Fernández et al., 2016; Senthilarasu et al., 2015). Results for air mass, AOD and precipitable water are show in Figure 5.

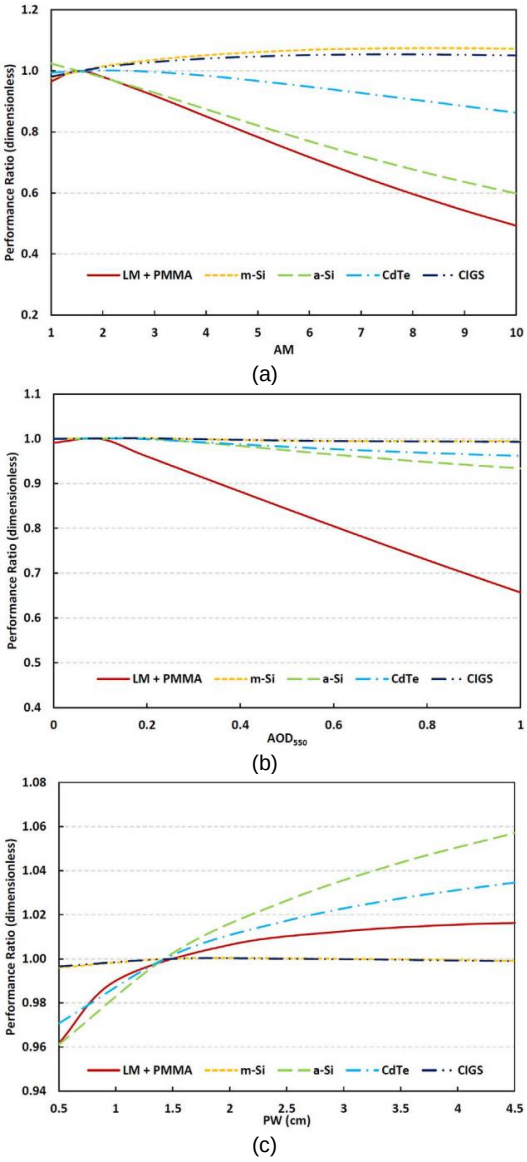


Figure 5 - Individual impact of AM (a), AOD (b) and PW (c) on different PV technologies' performance ratio, using the SMARTS model (Rodrigo et al., 2017).

2.3.2 Reference and Brazilian Spectral Distributions

Considering the relevance of spectral distribution on the power rating of PV devices, the solar community has agreed on a reference spectrum for the so-called standard test conditions (STC), used for testing PV modules. This spectrum was consolidated through the use of several spectral models and extensive research on the various extinction processes happening in the Earth's atmosphere (Bird et al., 1983; Gueymard et al., 2002; Hulstrom et al., 1985).

The most widely accepted spectral distribution to evaluate photovoltaic devices under STC is now the ASTMG-173-03 reference spectrum (ASTM, 2012) provided by the American Society for Testing and Materials (ASTM), obtained from the aerosol optical depth (AOD), precipitable water (PW), ozone column (O_3), carbon dioxide (CO_2), and average air mass (AM), from representative regions of the US.

However, the ASTM G173-03 spectrum is rarely reproduced in field conditions, where the main value of interest is not the efficiency under STC, but the electrical output under realistic operating conditions. Considering this, the PV community has extensively studied ways to better understand and quantify the impact of spectral changes on the output of the different solar devices.

Due to the high cost and complexity of maintenance and data acquisition, there are not many spectroradiometers available in Brazil, and there is currently no equipment performing continuous and long-term measurements for spectral characterization of the Brazilian territory. Simulation models for PV systems also do not faithfully represent spectral losses and/or gains, often neglecting this loss due to the complexity of modeling atmospheric dynamics and their impact on the solar spectrum (Duck and Fell, 2015). For these scenarios, an alternative is to obtain a spectral representation of a site using radiation transfer models (Myers and Gueymard, 2004), and atmospheric data originated from field measurements (Núñez et al., 2016) or satellite data (Amillo et al., 2015).

Table 1 shows the aerosol optical depth (AOD), precipitable water (PW), ozone column (O_3) and carbon dioxide (CO_2), and average air mass (AM) atmospheric values used to characterize the typical standard spectrum employed worldwide in the characterization of PV modules. Average values of Brazilian locations are also presented, showing the atmospheric differences between distinct regions of Brazil and the reference ASTM G173-03 spectrum. Using these inputs and the SMARTS model, characteristic spectra were defined for Brazil (Haag, 2012; Haag and Krenzinger, 2016).

Table 1 - Characteristic atmospheric parameters for distinct Brazilian locations and ASTM G173-03.The standard deviation for the concentration values of ozone (O_3), precipitable water (PW), and AOD are shown in parentheses (Haag, 2012).

Site	O_3 [DU]	PW [cm]	AOD	CO_2 [ppmv]
ASTM G173-03	343,8	1.42	0.084	370
Porto Alegre, RS	275.4 (9.26)	2.30 (0.24)	0.061 (0.028)	384
Petrolina, PE	286.5 (8.83)	3.24 (0.21)	0.040 (0.018)	381
Alta Floresta, MT	270.2 (9.48)	4.53 (0.24)	0.246 (0.11)	382
Manaus, AM	260.5 (9.75)	5.25 (0.15)	0.195 (0.068)	382

2.3.3 Spectral Response

The spectral response (SR) represents the conversion of the incident photons into electricity in a PV device and can be defined as the amperes generated per watt of incident light of a given wavelength (Rodrigo et al., 2017). In other words, the spectral response represents how the PV device responds to different wavelengths of the incident sunlight. Figure 6 shows the SR, or spectral absorption band, of some of the current most wide-spread PV materials.

Figure 7, on the other hand, presents the quantum efficiency (QE) of several PV materials. The quantum efficiency indicates the amount of current generated when irradiated by photons of a particular wavelength. The integral of the quantum efficiency over the entire solar electromagnetic spectrum gives the amount of current the cell will produce when exposed to solar radiation. The spectral response and the quantum efficiency are related through the formula shown in Eq. (4), where q is the electron charge, λ is the given wavelength, h is the Plank's constant and c is the speed of light. Eq. (4) essentially shows that quantum efficiency can be determined from the spectral response by replacing the power of the light at a particular wavelength with the photon flux for that wavelength.

$$SR = \frac{q\lambda}{hc} QE \qquad \text{Eq. (4)}$$

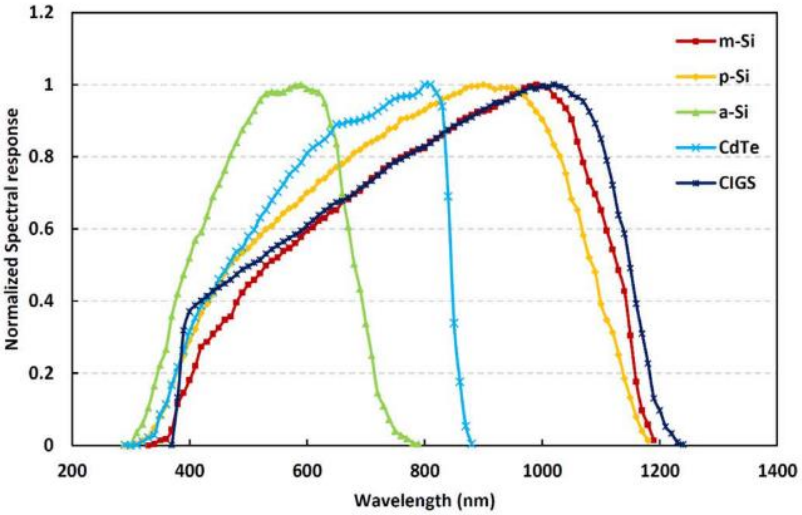


Figure 6 - Spectral response (SR) of the most wide-spread PV materials nowadays (Rodrigo et al., 2017).

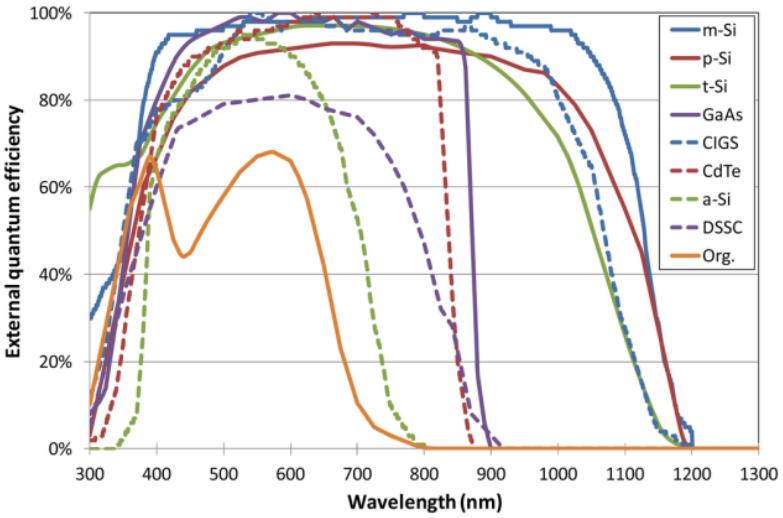


Figure 7 - Quantum efficiency (QE) for different PV technologies (Minnaert and Veelaert, 2014).

It can be observed that a-Si and CdTe technology present a narrower spectral response mainly at short wavelengths (blue-biased). In this way, these PV devices' performances will benefit in regions with blue-shifted spectral distributions (Gottschalg et al., 2005; Rüther et al., 2002). On the other hand, crystalline silicon-based technologies - mono- and multicrystalline silicon - have a redder spectral response, ranging up to 1200 nm.

2.3.4 Spectral Indexes

Rodrigo et al. (2017) classify the indexes used to quantify the effects of spectral distribution of sunlight on PV devices in PV device-independent and device-dependent. Indexes that do not depend on the PV device characterize the spectral distribution itself, therefore an index calculated for a specific spectral distribution is valid for all PV devices. PV device-dependent indexes, on the other hand, take into consideration the PV technology's spectral response, thus the indexes must be recalculated for different PV devices. This second category of indexes can be further classified into indexes that characterize the spectral impact on a PV device, indexes that characterize the relative spectral impact between two PV devices, and indexes that characterize the spectrum from multi-juntion solar cells. Figure 8 schematizes the commonly used spectral indexes according to the above-mentioned classification.

The Average Photon Energy (APE) is a PV device-independent index is defined as the total irradiance contained in the spectrum (integral of $E_G(\lambda)$) divided by the total photon flux density (integral of $\Phi_G(\lambda)$) (Jardine et al., 2002; Williams et al., 2003), as shown in Eq. (5). The photon flux density, in turn, is given by the relation between the spectral irradiance ($E_G(\lambda)$) and the product of the Plank's constant (h) by the speed of light (c), divided by the wavelength (λ), as shown in Eq. (6). The final units for APE, when using SI units, is electronvolts (eV).

$$APE = \frac{\int_{\lambda_1}^{\lambda_2} E_G(\lambda) d\lambda}{\int_{\lambda_1}^{\lambda_2} \Phi_G(\lambda) d\lambda} \qquad \text{Eq. (5)}$$

$$\Phi_G(\lambda) = \frac{E_G(\lambda)}{hc/\lambda} \qquad \text{Eq. (6)}$$

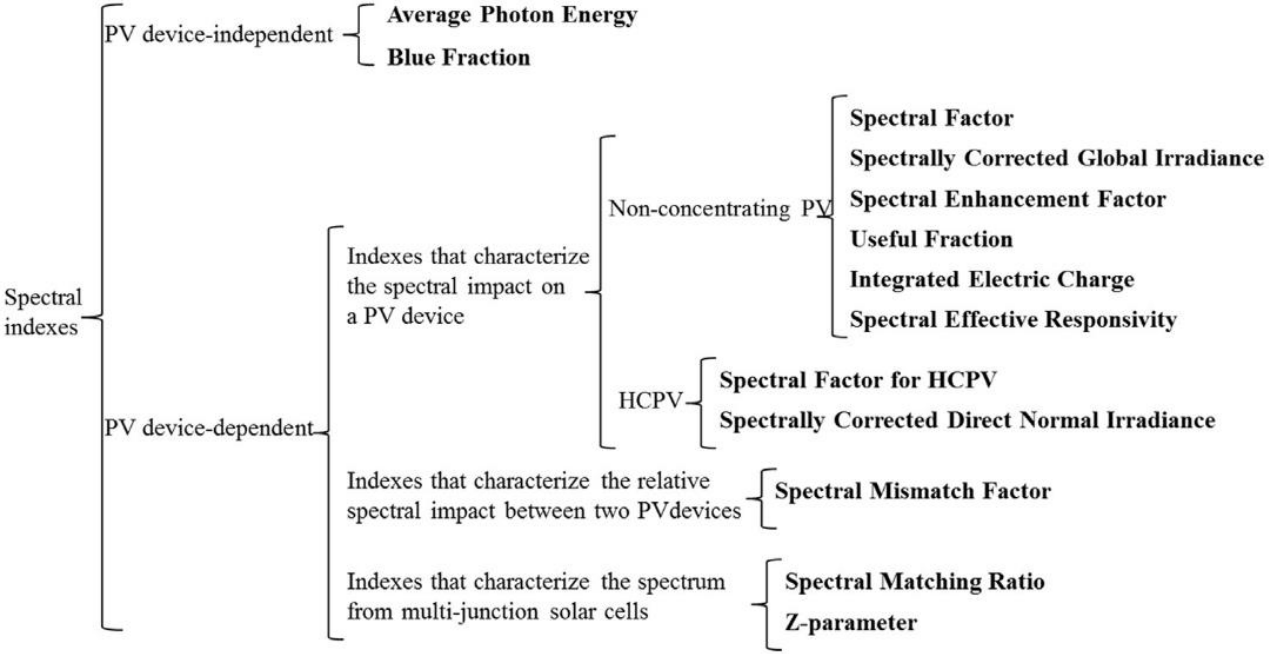


Figure 8 - Classification of indexes for quantifying spectral influences in photovoltaic systems (Rodrigo et al., 2017).

For the standard spectrum, considering wavelengths between 350 and 1050 nm, APE is 1.88eV. This index is related to the radiation's chromatic distribution, with low wavelength photons having less weight on the total photon flux density, meaning that low APE values correspond to "red-rich" spectral distributions. The disadvantage of the APE index is the need for measured/modeled spectral distribution and the vagueness between the index result and the actual spectral impacts.

Another PV device-independent index is the Blue Fraction (BF), which is simply the integral of the spectral irradiance contained in wavelengths below 650 nm divided by the total irradiance (Sutterlueti et al., 2008), as presented in Eq. (7). For the reference ASTM G173-03 spectrum, the resulting BF is 52% when integrating irradiance up to 1050 nm. This means that spectra with a BF above 52% can be considered "bluer" than the reference. The disadvantages of this index are the same as the ones stated for the APE index.

$$BF = \frac{\int_{\lambda<650} E_G(\lambda)d\lambda}{\int E_G(\lambda)d\lambda} \qquad \text{Eq. (7)}$$

The spectral factor (SF) index, is a dimensionless PV device-dependent coefficient that quantifies the spectral mismatch between the reference ASTM G173-03 spectrum ($E_G^*(\lambda)$) and the local spectrum ($E_G(\lambda)$), for a particular PV spectral response ($SR(\lambda)$) (Rodrigo et al., 2017). This index quantifies the actual spectral gains of a PV technology regardless of the reference irradiance sensor used. It must be noted that when correcting IV curve measurements or other irradiance-dependent parameters, the mismatch factor (MM) is a more suitable index, seeing that it correlates the spectral response of the reference sensor and the device under test as well as the reference and the measured spectra (Rodrigo et al., 2017). The formula for the spectral factor (SF) calculation is shown in Eq. (8).

$$SF = \frac{\int E_G(\lambda)SR(\lambda)d\lambda}{\int E_G^*(\lambda)SR(\lambda)d\lambda} \cdot \frac{\int E_G^*(\lambda)d\lambda}{\int E_G(\lambda)d\lambda} \qquad \text{Eq. (8)}$$

The Useful Fraction (UF) index, proposed by Gottschalg et al. (2005) and R. Gottschalg et al. (2003), is defined as shown in Eq. (9). This index correlates the irradiance present up to the PV device's absorption limits ($\lambda < \lambda_0$) to the total irradiance.

$$UF = \frac{\int_{\lambda<\lambda_0} E_G(\lambda)d\lambda}{\int E_G(\lambda)d\lambda} \qquad \text{Eq. (9)}$$

The index used for the spectral correction of peak-power measurements according to the IEC 60904-7 standard (International Electrotechnical Commission, 2008) is the spectral mismatch factor (MM), given by Eq. (10). The need for spectral correction of IV curve measurements rises from the mismatching between the spectral response of the reference device ($SR_{ref}(\lambda)$) and the device under test ($SR_{DUT}(\lambda)$), which results in different irradiances "seen" by the sample and the reference sensor. The mismatch factor, therefore, correlates the standard ASTM G173-03 ($E_{G173}(\lambda)$) and measured spectra ($E_G(\lambda)$) with the spectral responses of the sample ($SR_{DUT}(\lambda)$) and reference devices ($SR_{ref}(\lambda)$).

$$MM = \frac{\int E_G(\lambda)SR_{DUT}(\lambda)d\lambda}{\int E_{G173}(\lambda)SR_{DUT}(\lambda)d\lambda} \cdot \frac{\int E_{G173}(\lambda)SR_{ref}(\lambda)d\lambda}{\int E_G(\lambda)SR_{ref}(\lambda)d\lambda} \qquad \text{Eq. (10)}$$

The mismatch factor equals the SF index when using an ideal device with a flat spectral response over the analyzed wavelength interval as a reference. The most common device that fits this description is a pyranometer, which operates under a thermoelectric rather than a photoelectric principle.

3 METHOD

3.1 MEASUREMENT SETUP

In order to evaluate the methods presented in this study, measured spectral data among other environmental parameters were required. Long-term data and instantaneous measurements were used to evaluate distinct methods used in two particular scenarios where spectral impacts must be accounted for: instantaneous measurements for IV curve correction and long term analysis.

The long-term measured data used in this study were obtained from the solar measurement station located at the Fotovoltaica-UFSC laboratory (www.fotovoltaica.ufsc.br), in the city of Florianópolis-SC, Brazil (27°S, 48°W). The solar measurement station is shown in Figure 9, and a list of all of the sensors installed can be found in . The spectral measurements at this station are made using a stationary EKO MS-711 spectroradiometer (sensor number 8 in Figure 9 and Table 2) in a one-minute basis within the 300-1100 nm wavelength range, as presented in Table 2. Irradiance data for Florianópolis-SC were also acquired using a Kipp & Zonen SMP22-V pyranometer (sensor number 7 in Figure 9 and Table 2), together with relative humidity and ambient temperature, which were measured using a Vaisala HMP155A (sensor number 10b in Figure 9 and Table 2).

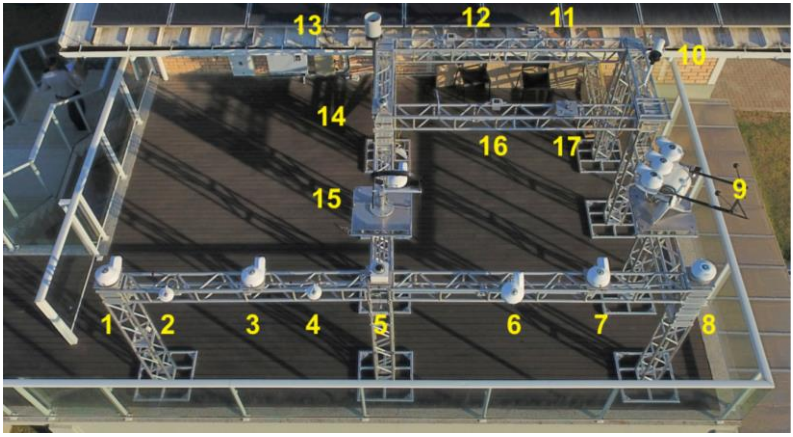


Figure 9 - Solar measurement station located at the Fotovoltaica-UFSC research laboratory in Florianópolis-SC, Brazil (27°S, 48°W), numbered according to Table 2.

Table 2 - List of sensors installed at the Fotovoltaica-UFSC research laboratory in Florianópolis-SC, Brazil (27°S, 48°W), numbered according to Figure 9.

	Measurement	Model	Manufacturer		Measurement	Model	Manufacturer
1	*Ultraviolet*	*CUV-5-V*	*Kipp & Zonen*	*9e*	*Global Tilted (1-Axis)*	*SMP11-V*	*Kipp & Zonen*
2	*Global Tilted*	*SMP6*	*Kipp & Zonen*	*9f*	*Global Tilted (2-Axis)*	*SMP11-V*	*Kipp & Zonen*
3	*Global Horizontal*	*SMP11-V*	*Kipp & Zonen*	*10a*	*Wind*	*WINDSONIC1*	*GILL*
4	*Global Tilted*	*SMP11*	*Kipp & Zonen*	*10b*	*RH & Temperature*	*HMP155A*	*VAISALA*
5	*All- Sky Camera*	*SRF-02*	*EKO*	*11*	*Global Horizontal*	*Si-02-PT100*	*IMT*
6	*Global Tilted*	*SMP11-V*	*Kipp & Zonen*	*12*	*Global Tilted (Clean)*	*Si-02-PT100*	*IMT*
7	*Global Horizontal*	*SMP22-V*	*Kipp & Zonen*	*13*	*Pluviometer*	*TB4-L*	*HS*
8	*Solar Spectrum*	*MS-711*	*EKO*	*14*	*Global/Diffuse*	*SPN1*	*Delta-T*
9a	*IR & long-wave*	*SGR4-V*	*Kipp & Zonen*	*15*	*Diffuse Horizontal*	*SMP11*	*Kipp & Zonen*
9b	*Global Horizontal*	*SMP22-V*	*Kipp & Zonen*	*16*	*Global Tilted (Soiled)*	*Si-02-PT100*	*IMT*
9c	*Diffuse Horizontal*	*SMP22-V*	*Kipp & Zonen*	*17*	*PAR*	*PQS-1*	*Kipp & Zonen*
9d	*Direct Normal*	*SHP1-V*	*Kipp & Zonen*				

Furthermore, instantaneous spectral measurements were made in the field at a utility-scale PV power plant in Assu-RN, located in the Brazilian Northeast (5°S, 37°W), using a portable EKO MS-720 spectroradiometer, as shown in Figure 10. This device allows measurements within the 350-1050 nm wavelength range, as presented in Table 3.



Figure 10 - On-site spectral measurements made with the EKO MS-720 portable spectroradiometer in Assu-RN, Brazil (5°S, 37°W).

Table 3 - Main specifications of the spectroradiometers used to obtain spectral data for the analysis.

	MS-711	**MS-720**
Type	stationary	portable
Wavelength range	300 - 1100 nm	350 - 1050 nm
Optical resolution FWHM	< 7 nm	< 10 nm
Wavelength accuracy	+/- 0.2 nm	< 0.3 nm

Annual environmental data for the application of direct methods for spectral impact estimation at the Assu-RN site were acquired from a local weather station. The data comprehends a full year of consecutive measurements (Jan.-Dec. 2016) with a ten-minute time resolution (as required of new PV power plants to present in order to be eligible to take part in Brazilian energy auctions (EPE, 2017)).

3.2 SATELLITE DATA ACQUISITION

For the application of the proposed method, environmental parameters were obtained from publicly available data through the Giovanni online platform, a tool that displays data from NASA satellites directly on the internet (NASA, n.d.). The use of satellite data to model spectral behavior and analyze spectral impacts on PV technologies was previously proposed by Haag (2012).

The Giovanni platform allows the user to research parameters, choose a satellite among the many available, select a time period and location, and plot the data in a very straightforward manner. After plotting, it is also possible to export the data as an image (chart format) or a comma-separated-values file (.csv, in table format).

The satellites used in this study for the long-term analysis of spectral impacts in Florianópolis- and the corresponding parameters and resolutions obtained from each of them can be found in Table 4.

For the Assu site, precipitable water data were obtained to correlate the spectral factor calculated for on-site measurements with different atmospheric conditions. The sources used to obtain data for this site are also presented in Table 4, along with their respective units, temporal and spatial resolutions.

Table 4 - Data sources within NASA Giovanni platform used in the present study.

Source	Measurement	Units	Temporal Resolution	Spatial Resolution	Site
MODIS-Terra	Aerosol Optical Depth @ 550nm	-	Daily	1°	Florianópolis
AIRS	Carbon Dioxide Mole Fraction	ppmv	Monthly	2° x 2.5°	Florianópolis
MODIS-Terra	Precipitable Water Vapor	cm	Daily	1°	Florianópolis
OMI	Ozone Total Column	DU	Daily	0.25°	Florianópolis
MERRA-2	Precipitable Water Vapor	cm	Hourly	0.5° x 0.625°	Assu

3.3 SOLAR GEOMETRY DATA

Relative air mass data were retrieved for both locations using NREL's Measurement and Instrumentation Data Center (MIDC) solar position (SOLPOS) calculator (NREL, n.d.). The SOLPOS calculator computes the solar position and intensity from time and place according to the user's inputs of latitude, longitude, time zone, surface pressure and ambient dry-bulb temperature, among other optional inputs. The user must also input the time period and interval of the output and the desired parameters to be calculated.

The calculated relative air mass was used for SMARTS spectra modeling, while pressure-corrected air mass was used in the application of direct methods for calculation of SF. The surface pressure values needed for the pressure-corrected air mass computation were the periods' measured data average (from the solar measurement station shown in Figure 9) and satellite data average (from the Giovanni platform) for Florianópolis-SC and Assu-RN, respectively.

3.4 SPECTRA MODELING

The SMARTS (Simple Model of the Atmospheric Radiative Transfer of Sunshine) is a FORTRAN code that aims to model the spectral distribution of solar irradiance at a given location and environmental conditions. The model allows the user to input several parameters such as air mass, precipitable water, AOD, among many others, to model the

spectral conditions at a certain location and time (Gueymard, 2006, 1995; Myers and Gueymard, 2004). The SMARTS model is often used to model spectral characteristics in order to evaluate the spectral impacts of such spectrum on a given PV system (Betts, 2004; Haag, 2012; Haag and Krenzinger, 2016; Myers et al., 2002; Nelson et al., 2013; Stark and Theristis, 2015).

The inputs for the SMARTS model used in the present study for Florianópolis are shown in Table 5. For precipitable water, ozone vertical column, carbon dioxide concentration and AOD, satellite data according to Table 4 for the day/month were used. As previously mentioned, when data were unavailable an interpolation or extrapolation was made with the available data points in order to fulfill gaps.

3.5 SPECTRAL FACTOR

As previously mentioned, there are several indexes for quantifying the effects of different spectral distributions of light on PV technologies. Some of these indexes characterize the spectral distribution of light itself, such as the blue fraction and APE (average photon energy), while others relate a given spectral distribution with the standard spectrum and a specific spectral response (spectral factor, useful fraction, etc.) or even correlate the relative spectral impacts between two PV devices (spectral mismatch factor) (Rodrigo et al., 2017).

The focus of this study is the spectral factor (SF), a dimensionless coefficient that quantifies the spectral mismatch between the reference ASTM G173-03 spectrum ($E_G^*(\lambda)$) and the local spectrum ($E_G(\lambda)$), for a particular PV spectral response ($SR(\lambda)$) (Rodrigo et al., 2017). This index was chosen because it quantifies the actual spectral gains of a PV technology regardless of the reference irradiance sensor used. It must be noted that when correcting IV curve measurements or other irradiance-dependent parameters, the mismatch factor (MM) is a more suitable index, seeing that it correlates the spectral response of the reference sensor and the device under test as well as the reference and the measured spectra (Rodrigo et al., 2017). The formula for the spectral factor (SF) calculation was previously shown in Eq. (8).

Because the variables shown in Eq. (8) are discrete sets of data with distinct wavelengths, an interpolation between points was necessary in order to have all datasets in the same wavelength bases. The trapezoidal rule was employed to evaluate the definite integrals.

The spectral responses used in the calculation of the spectral factor are shown in Figure 11 for mc-Si and new generation CdTe in red (wider,

red-shifted curve) and blue (narrower, blue-shifted curve) respectively. The spectral responses used in this study were provided by a reference cell manufacturer - for mc-Si - and a module manufacturer - for new generation CdTe (First Solar, 2017).

Table 5 - Inputs for the SMARTS model used in the present study for Florianópolis-SC, Brazil (27°S, 48°W).

Card #	Card Name	Parameter	Value	Unit
Card 2	Site Pressure	Altitude	0	km
		Height	0	km
		Latitude	-27.430706	°
Card 3	Atmosphere	Reference Atmosphere	SubTropical Summer	-
Card 4	Water Vapor	Precipitable Water	Satellite Data	cm
Card 5	Ozone	Ozone Vertical Column	Satellite Data	atm-cm
Card 6	Gaseous Absorption	Use Defaults from Selected Atmosphere		
Card 7	Carbon Dioxide	Carbon Dioxide Concentration	Satellite Data	ppmv
Card 7a	Extraterrestrial Spectrum	Gueymard 2004		
Card 8	Aerosol Model	Rural		
Card 9	Turbidity	Aerosol Optical Depth at 550nm	Satellite Data	-
Card 10	Albedo	Green Grass Denver		
Card 10b	Tilt Albedo	Bypass		
Card 11	Spectral Range	Minimum	280	nm
		Maximum	1200	nm
		Solar Constant	1366.1	W/m^2
		Solar Constant Distance Correction factor	1	-
Card 12	Output	Create .OUT and .EXT files, include spectral results in .EXT file only		
		Spectral range to be printed	280-1200	nm
		Spectral Results	Global horizontal irradiance	
Card 13	Circumsolar	Bypass		
Card 14	Smoothing Filter	Bypass		
Card 15	Illuminance	Bypass		
Card 16	UV	Bypass		
Card 17	Solar Geometry	Input relative Air Mass	Calculated	-

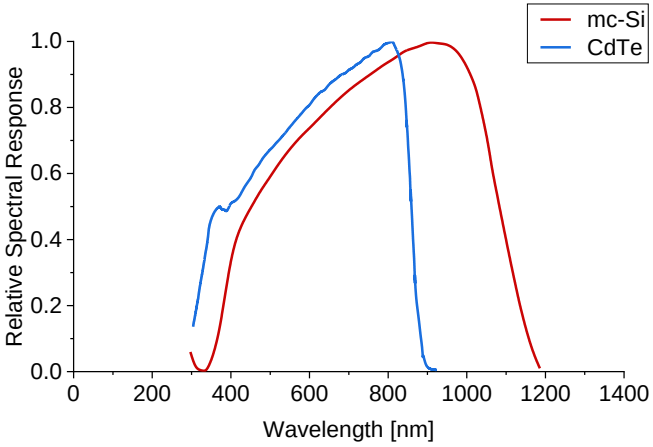


Figure 11 - Spectral responses for mc-Si (wider, red-shifted curve) and new generation CdTe (narrower, blue-shifted curve) used in the computation of spectral indexes in this thesis.

On Figure 11 it can be observed that the spectral response of mc-Si comprehends wavelengths of up to 1200 nm, while CdTe has a narrower response, ranging from 300 nm to 900 nm only. The measuring range of the spectroradiometers used in this study go up to 1050 and 1100 nm, for MS-720 and MS-711 respectively, encompassing all of the CdTe spectral response range, but only part of multicrystalline silicon's, introducing great uncertainty in the analysis (Dirnberger et al., 2015c).

The total uncertainty associated with the calculation of the SF can be estimated using the methodology presented by Dirnberger and Reise (2015), where uncertainties ranging from 0.9% to 1.8% were found. This analysis will not be presented at this time, but it is important to understand the sources of uncertainty and how they affect SF differently for mc-Si and CdTe.

The uncertainty associated with the spectra measurements ($E_G(\lambda)$) can be traced back to the spectroradiometers' calibration, cosine response, linearity, wavelength accuracy and temperature dependence. The reference spectral distribution ($E_G^*(\lambda)$) is a definition and, therefore, has no uncertainty. The spectral response of the evaluated PV devices also has an uncertainty associated with its measurement, with its temperature dependence caused by the semiconductor's bang gap's temperature dependence (Litjens, 2013), and with the use of spectral results of one

specific PV device for other devices employing that same PV technology. In addition, it has been shown that the magnitude of the spectral index itself is not significant for its uncertainty, but how similar the evaluated spectrum and the reference spectrum are is very relevant (Field and Emery, 1993; Hohl-Ebinger and Warta, 2011; King et al., 2002).

Other sources of uncertainty in the present analysis are derived from the numerical methods employed: the interpolation carried out in order to have all datasets in the same wavelength bases and the trapezoidal rule used in the computation of the definite integrals.

3.6 SF ESTIMATION

3.6.1 SMARTS + Giovanni Method

The proposed method for estimating the spectral factor consists of three basic steps:

1. Acquisition of environmental parameter values for a specific location and time from NASA satellites' database through the Giovanni online platform (NASA, n.d.);
2. Modeling of the local spectrum using the SMARTS 2.9.5 software;
3. Calculation of the spectral factor (SF) in order to quantify the spectral mismatch impact of the modeled spectrum on a specific PV technology.

This method allows the calculation of spectral impacts without the need for in loco measurements. From the spectra modeled through the SMARTS model, the spectral factor is calculated for two PV technologies: multicrystalline silicon (mc-Si) and new generation cadmium telluride (CdTe), using the spectral responses shown in Figure 11. Considering that the proposed methodology involves the modeling of spectra, it can also be applied in the calculation of other spectral indexes, such as the mismatch factor (MM) and the APE (average photon energy).

3.6.2 Direct Methods

Several authors have also proposed direct methods for the quantification of spectral impacts on PV systems (King et al., 2004, 1997; Lee et al., 2015a, 2015b; Nelson et al., 2013). These direct methods are empirical correlations that exempt the need of a local spectrum and the use of integrals in the computation of the spectral impact on a PV system. In this study, three of these empirical correlations will also be applied to measured data to assess their accuracy for South Brazil Florianópolis' warm and humid subtropical climate.

The most common direct method for quantifying the spectral impact on a PV system is the Sandia spectral correction method, developed by Sandia National Labs. The method consists of an empirical fourth-order polynomial expression shown in Eq. (11), where AM_a is the absolute pressure-corrected air mass and a_0, a_1, a_2, a_3 and a_4 are the Sandia coefficients (King et al., 2016, 2004, 1997; King and Eckert, 1996). The method was intended to be applicable to all PV technologies; however, it only takes into consideration the absolute pressure-corrected optical air mass (AM_a), which is the major environmental variable affecting mc-Si spectral gains, but the same is not true for CdTe modules. For this reason, the correlation works well for crystalline silicon based technologies, but not adequately for CdTe (Duck and Fell, 2015; Lee and Panchula, 2016).

$$SF_{AM} = a_0 + a_1 AM_a + a_2 AM_a^2 + a_3 AM_a^3 + a_4 AM_a^4 \qquad \text{Eq. (11)}$$

As previously mentioned, thin-film CdTe has a blue-shifted and narrow spectral response (up to 900 nm) and therefore has its performance increased by environmental conditions that absorb irradiant light outside its spectral response range. Water vapor is the major environmental variable that affects these wavelengths outside CdTe spectral response (above 900 nm), meaning that in conditions where precipitable water is in abundance in the atmosphere, CdTe PV modules have a significant boost in performance. This is where the second direct method evaluated in this study comes into place: the precipitable water (Pwat) method. Given that precipitable water (U_W) is the main driver for CdTe spectral impacts, Nelson et al. (2013) proposed a method fitted for CdTe modules that consists of an empirical correlation between spectral factor and precipitable water only. Eq. (12) shows the precipitable water method correlation with the coefficients for new generation CdTe.

$$SF_{P_{wat}} = 1.266 - 0.0913\exp(1.1987(U_W + 0.5)^{-0.21}) \quad \text{Eq. (12)}$$

The above-mentioned direct methods for spectral impact calculation can only be applied with satisfactory results to specific PV technologies. Aiming to attend to both CdTe and mc-Si modules, Lee and Panchula (2016) proposed a two-parameter empirical method (2-parameter). The method uses both absolute pressure-corrected air mass (AM_a) and precipitable water (U_W) as inputs, as shown in Eq. (13). The coefficients b_0 through b_5 for both mc-Si and new generation CdTe were obtained from (Lee and Panchula, 2016) and are shown in Table 6.

$$SF_{2\text{-}par} = b_0 + b_1 AM_a + b_2 U_W + b_3\sqrt{AM_a} + b_4\sqrt{U_W} + b_5\frac{AM_a}{\sqrt{U_W}} \quad \text{Eq. (13)}$$

Table 6 - 2-parameter method coefficients for mc-Si and CdTe obtained from (Lee and Panchula, 2016).

	b_0	b_1	b_2	b_3	b_4	b_5
mc-Si	0.8409	-0.02754	-0.00792	0.1357	0.03802	-0.002122
CdTe	0.7946	-0.05423	-0.01319	0.1724	0.08372	-0.004376

For sets of data that did not include this parameter, precipitable water values (U_W) were estimated from relative humidity (RH, given as a percentage) and ambient temperature (T_a, in Kelvin) measurements from the solar measurement stations using Eq. (14) (First Solar, n.d.; Gueymard, 1994).

$$U_W \approx 0.1\left(0.4976 + 1.5265\frac{T_a}{273.15} + e^{13.6897\frac{T_a}{273.15} - 14.9188\left(\frac{T_a}{273.15}\right)^3}\right) \times \left(216.7\frac{RH}{100T_a}e^{22.33 - 49.14\frac{100}{T_a} - 10.922\left(\frac{100}{T_a}\right)^2 - 0.39015\frac{T_a}{100}}\right) \quad \text{Eq. (14)}$$

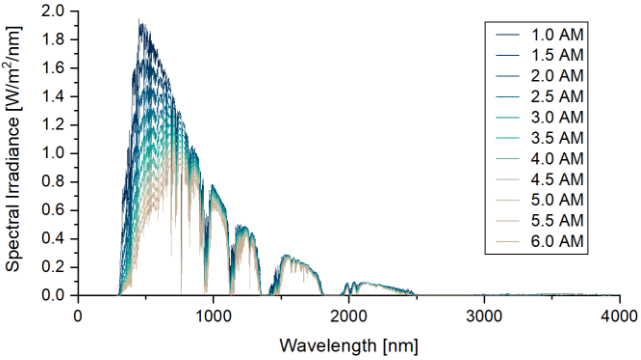
4 PRELIMINARY RESULTS

This section presents the preliminary results obtained in this thesis up to the present time.

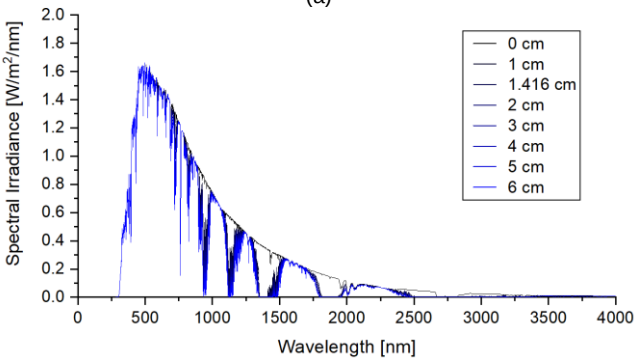
4.1 IMPACT OF ENVIRONMENTAL VARIABLES ON THE LOCAL SPECTRUM

The main environmental variables that affect the spectral distribution of light are air mass (AM), precipitable water (PW), aerosol optical depth (AOD), ozone (O_3) and carbon dioxide (CO_2). The impact of these parameters on the spectrum was evaluated through the simulation of the standard ASTM G173-03 spectrum using the SMARTS model, with only one of the above-mentioned parameters being varied. The wavelength range simulated was from 280 nm to 4000 nm and results can be found in Figure 12. The ranges in which each individual parameter was varied was found to be representative of real conditions around the globe and had been previously used in other studies as well (Betts, 2004; Haag, 2012; Lee and Panchula, 2016; Stark and Theristis, 2015).

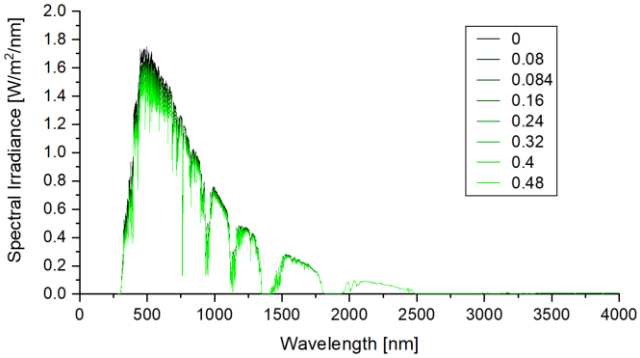
The air mass values were varied from AM 1.0 to 6.0, with 0.5 intervals, and it was the variable that had the greatest impact on the simulated spectra, especially within the visible light range (400-750 nm). Precipitable water was varied from 1 to 6 cm in 1 cm intervals and it showed to have a great impact on higher wavelengths (infrared), especially around 950 nm and 1150 nm. For AOD values the range used was from 0 to 0.48, with 0.08 intervals; the impact of this variable is more noticeable in the shorter wavelengths. For ozone, the simulated interval was from 0.00 to 0.50 atm-cm, with 0.05 atm-cm increments, and the greater variation on the simulated spectra was observed within 500 nm and 700 nm. Carbon dioxide was varied from 200 to 600 ppmv and no significant impacts were observed.


Spectral Irradiance [W/m²/nm]
Wavelength [nm]
1.0 AM
1.5 AM
2.0 AM
2.5 AM
3.0 AM
3.5 AM
4.0 AM
4.5 AM
5.0 AM
5.5 AM
6.0 AM

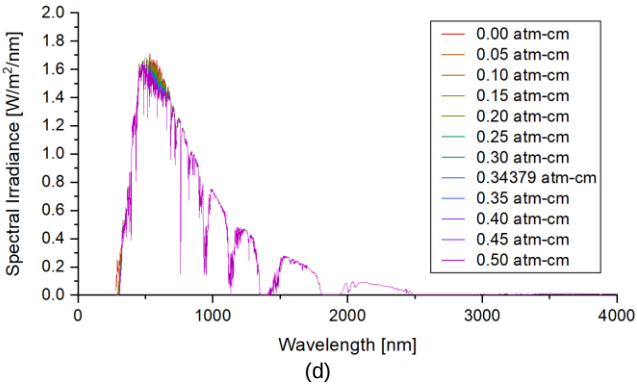
(a)


Spectral Irradiance [W/m²/nm]
Wavelength [nm]
0 cm
1 cm
1.416 cm
2 cm
3 cm
4 cm
5 cm
6 cm

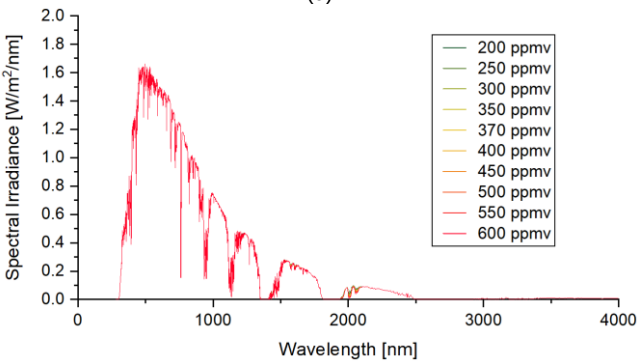
(b)


Spectral Irradiance [W/m²/nm]
Wavelength [nm]
0
0.08
0.084
0.16
0.24
0.32
0.4
0.48

(c)



(d)



(e)

Figure 12 - Impact of the main environmental variables on the local spectrum: (a) air mass (AM); (b) precipitable water (PW); (c) aerosol optical depth @ 550nm (AOD_{550}); (d) ozone (O_3); and (e) carbon dioxide (CO_2).

The results presented in Figure 12 must be translated into spectral impacts on PV technologies in order to assess which variables would affect the most the performance of PV systems, seeing that a major change in spectrum might be irrelevant for one technology but might result in big changes in performance for a different one. Figure 13 shows the spectral factors calculated for both mc-Si and CdTe according to Eq. (8) for the same ranges of values as Figure 12 for AOD, precipitable water and air mass.

It can be seen on Figure 13 (a) that AOD has a very small impact on the spectral factor for CdTe and even smaller for mc-Si. Precipitable water, on the other hand, has a more significant impact on CdTe's SF, while having nearly no effect on mc-Si's, as shown in Figure 13 (b). This

result was expected once precipitable water lowers the spectral content outside CdTe's spectral response range (see Figure 11 and Figure 12 (b)), which in turn yields a spectral advantage for this PV technology. Air mass, shown in Figure 13 (c), has a great positive impact on mc-Si and very negative impact on CdTe. On Figure 12 (a), it could be observed that increased air mass values decreased the spectral irradiance content for shorter wavelengths, meaning that high air mass values result in red-shifted spectra, which in turn is an advantage for mc-Si - because of its broad spectral response - and a spectral disadvantage for CdTe.

4.2 SATELLITE ATMOSPHERIC DATA

Figure 14 shows the downloaded environmental data for Florianópolis. Precipitable water, AOD and ozone data were downloaded from September 2017 until January 2018 (Figure 14 (a), (b) and (c), respectively), to observe the parameters variation in that time frame.

Linear interpolation between known points of data was used to obtain data needed for days in which they were unavailable. Due to lack of carbon dioxide data (Figure 14 (d)) for the analyzed period for the selected satellite, the time period downloaded for this parameter was extended and a monthly trend could be observed over the past seven years; this trend was then used to estimate CO_2 values for the evaluated period. It must be noted that precipitable water for this site ranged from approximately 0.5 cm to around 2.2 cm in the evaluated period. AOD values varied from 0.07 to 0.43 and ozone values from 240 atm-cm to 380 atm-cm. CO2 values have increased from 387 ppmv to 406 ppmv in the past seven years, although no significant change was observed for short time period windows.

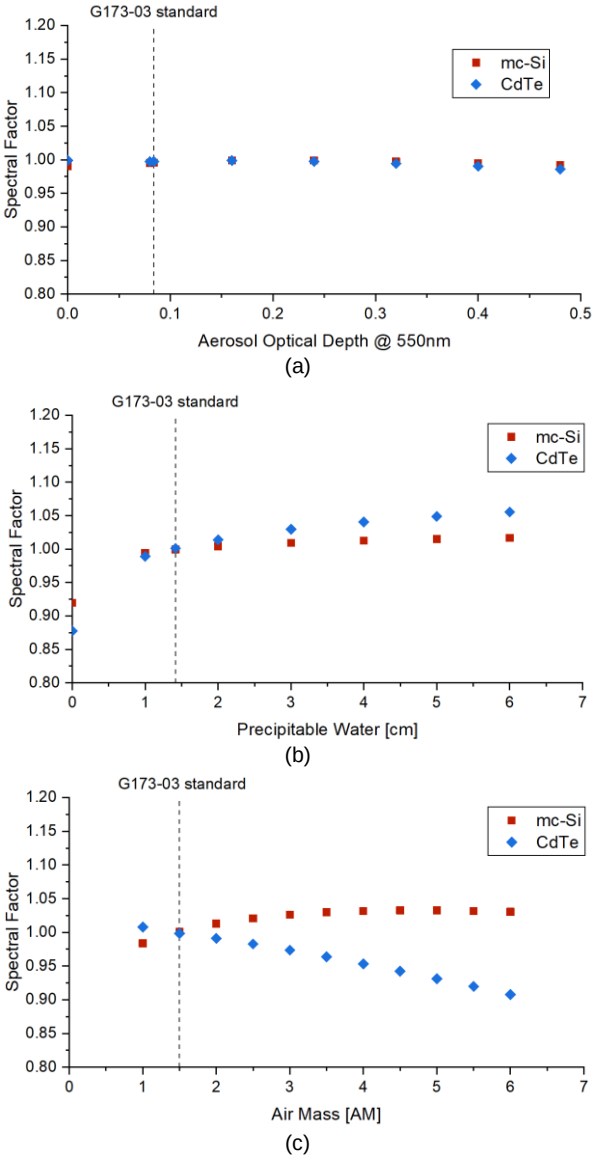


Figure 13 - Impact of (a) AOD, (b) precipitable water and (c) air mass on the spectral factor for mc-Si (red squares) and new generation CdTe (blue diamonds).

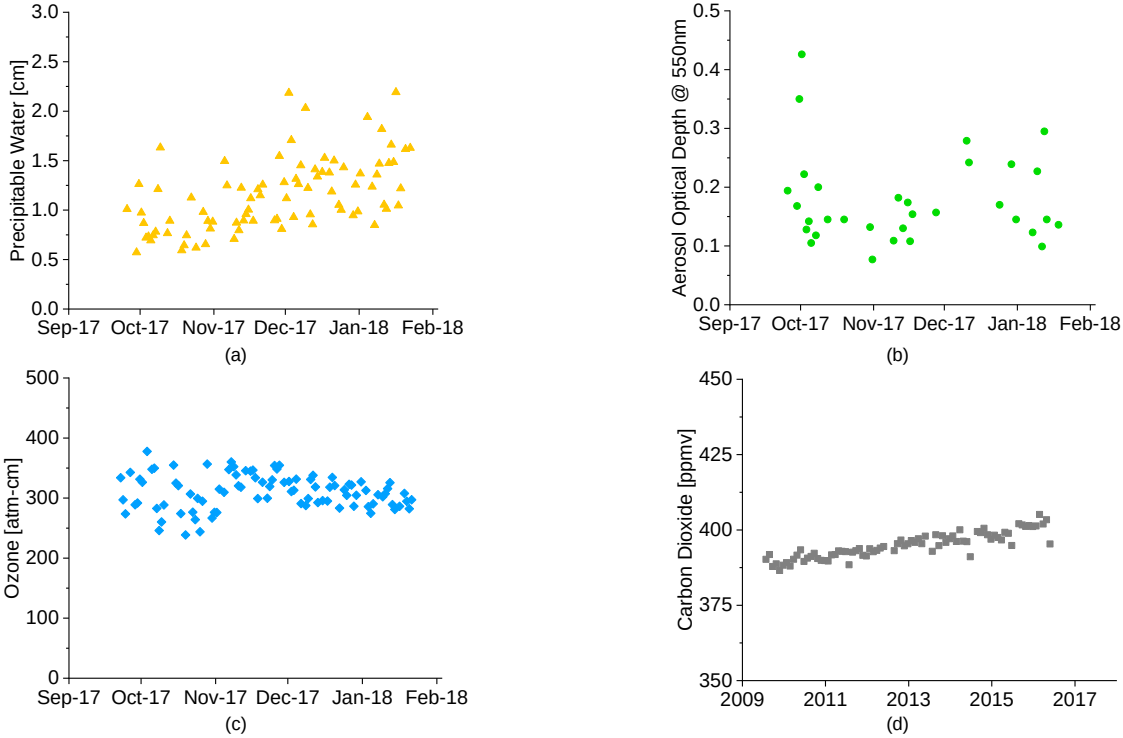


Figure 14 - Environmental parameters for Florianópolis-SC, Brazil (27°S, 48°W) obtained from the Giovanni platform (NASA, n.d.). (a) precipitable water (b) AOD @ 550nm (c) O_3 and (d) CO_2.

4.3 SPECTRAL IMPACTS ON MC-SI AND CDTE IN TWO DISTINCT REGIONS OF BRAZIL

The impacts of measured spectra for two distinct regions of Brazil were also calculated in this study using the spectral factor metric previously presented in Eq. (8). Measured data were obtained with a portable EKO MS-720 spectroradiometer for Assu-RN (5°S, 37°W) and with a stationary EKO MS-711 spectroradiometer for Florianópolis-SC (27°S, 48°W), as described in the prior section. Florianópolis is located on the coast of the South region of Brazil and has a warm humid subtropical climate (Cfa in the Köppen-Geiger climate classification (Alvares et al., 2013; Peel et al., 2007)). Assu-RN, on the other hand, is situated in the northeast of Brazil, about 60km from the coast; its climate is hot and dry semi-arid (Bsh in the Köppen-Geiger climate classification (Alvares et al., 2013; Peel et al., 2007)).

Figure 15 shows measured spectra for Florianópolis-SC and Assu-RN, along with the reference ASTM G173-03 spectrum and the calculated Blue Fraction (BF) index. In order to truly compare the spectral distributions of the sites, spectra were normalized to match the same irradiance level as the reference spectrum for the measured wavelength range. The Blue Fraction (BF) was calculated using previously shown Eq. (7).

By definition, the BF of the G173-03 spectrum is 52%, however, only the wavelengths within the spectroradiometers' range (see Table 3) were considered for this analysis. Figure 15 shows that both sites present bluer spectra than the reference ASTM G173-03 (55% for Florianópolis and 57% for Assu), meaning CdTe has a spectral advantage on these regions over mc-Si.

The spectral factor results for both mc-Si and new generation CdTe are shown in Figure 16 (a) for Florianópolis-SC. The spectral measurements for the computation of these SF were taken at the solar measurement station at Fotovoltaica-UFSC in Florianópolis on a one-minute basis and averaged into 15-minute intervals on October 28th, 2017. In Figure 16 (b), the same results are presented for 89 spectral measurements made between November 21st and December 15th, 2017 in Assu. Pressure-corrected air mass values are also shown for both sites. Precipitable water values (U_W) for Florianópolis were estimated from relative humidity (RH, given as a percentage) and ambient temperature (T_a, in Kelvin) measurements from the solar measurement station shown in Figure 9 using Eq. (14). Precipitable water values for Assu were

obtained from the Giovanni online platform using the MERRA-2 satellite with hourly resolution data.

For Florianópolis (Figure 16 (a)), a correlation between SF for mc-Si and air mass values is noticeable, with this PV technology reaching SF values above 1 (representing gains) for early morning and late afternoon (air mass values above 3) and SF values below 1 (representing spectral losses) during most of the day. Overall, SF for mc-Si varied from 0.98 to 1.00 for instants in which irradiance was greater than 200 W/m^2 in the analyzed day, and the irradiance-filtered (only measurements where irradiance was above 200 W/m^2 were considered) and weighted average obtained for this technology was 0.98. The average precipitable water content for the analyzed day was 2.43 cm, well above the 1.416 cm of the standard spectrum. In general, new generation CdTe SF values ranged from 1.00 to 1.02 for irradiance levels above 200 W/m^2 on October 28th, 2017 in Florianópolis-SC, and the irradiance-filtered and weighted SF obtained was 1.01.

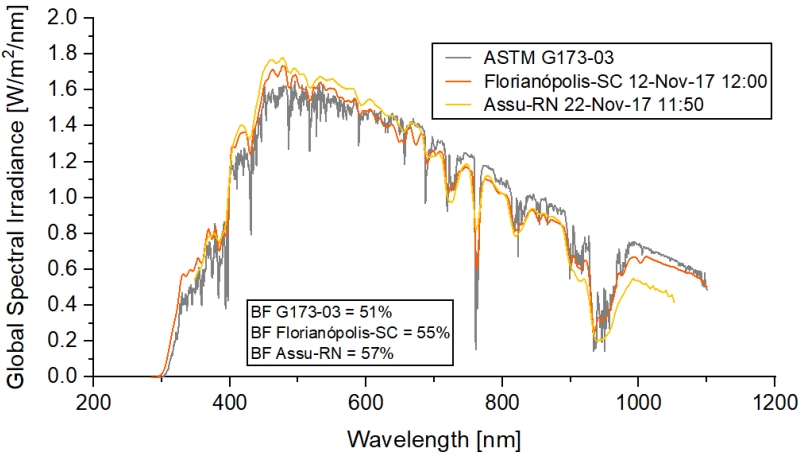


Figure 15 - Comparison between the reference ASTM G173-03 spectrum (gray line, 52% BF) and spectra measured for Florianópolis-SC, Brazil (27°S, 48°W) on November 12th, 2017 at 12:00 (orange line, 55% BF) and for Assu-RN, Brazil (5°S, 37°W) on November 22nd, 2017 (yellow line, 57% BF). Spectra were normalized to match the reference spectrum irradiance over the measured wavelengths.

The measurements for Assu-RN were done in different times of the day throughout several days, and ordered according to the local time, so that a daily trend could be observed. For precipitable water (yellow triangles), the values varied from day to day, and that is why there is a cloud of points instead of a set of continuous points of data for this variable. For this site, a stronger correlation between air mass and SF for both technologies could be observed. For air mass values greater than 2 there is an abrupt increase in SF for mc-Si and a 4% decrease in SF for new generation CdTe. These results corroborate the results shown in Figure 13 (c) obtained from simulated ASTM G173-03 spectra with various AM values. The SF values for mc-Si ranged from 1.00 to 1.06 during the evaluated period, with an irradiance-filtered and weighted average of 1.02. The irradiance-filtered and weighted average falls closer to the minimum values of SF for mc-Si because its higher values occurred during the end of the day, when there is high AM but low irradiance. For new generation CdTe, SF ranged from 1.06 to 1.10, with an irradiance-weighted average of 1.09, showing that this technology has great spectral advantages in this area. The high SF values can be associated with low AM found in low-latitude regions and the higher precipitable water content of the region, which averaged 3.42 cm for the evaluated period, almost 1 cm more than the average value for the day analyzed in Florianópolis, which was 2.43 cm. It is important to highlight that both regions still presented higher precipitable water values than the standard ASTM G173-03 spectrum (1.416 cm), making the spectra at these regions very favorable for CdTe PV modules.

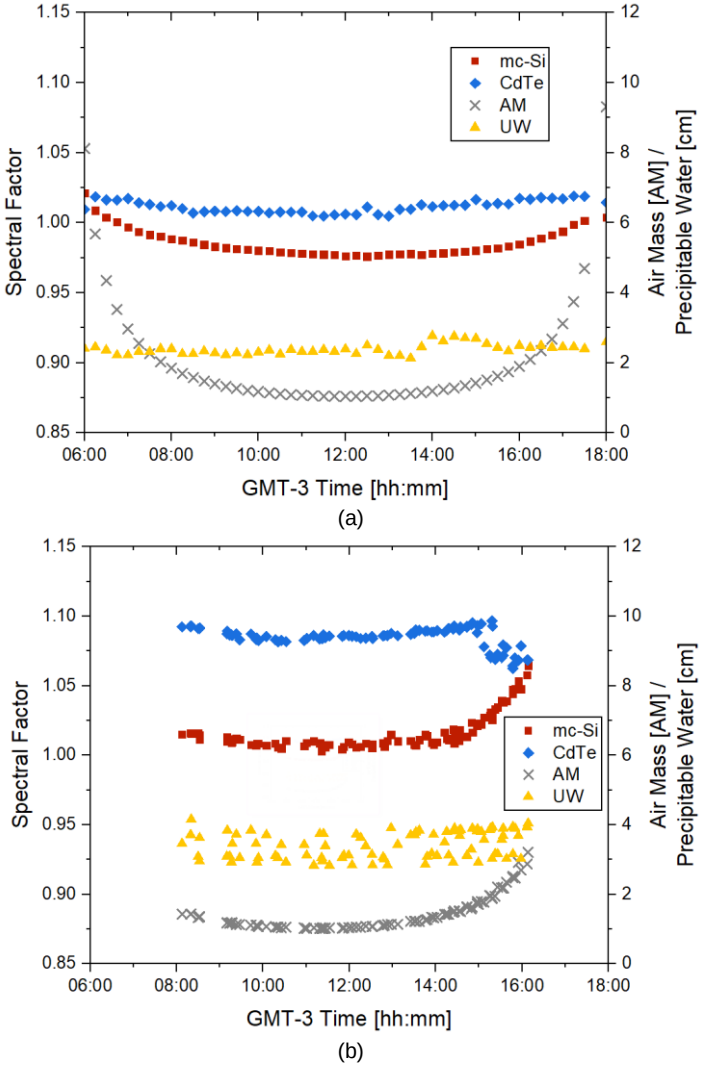


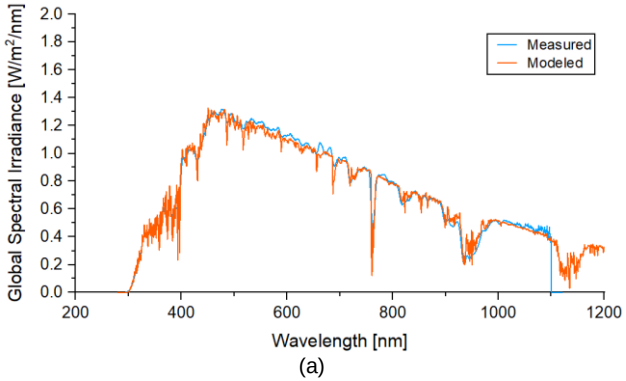
Figure 16 - Spectral factor for mc-Si (red squares) and new generation CdTe (blue diamonds) calculated for 15-minute-averaged spectral measurements during a clear day (Oct. 28th, 2017) in Florianópolis-SC, Brazil (27°S, 48°W) (a) and for several spectral measurements for clear days (Nov. through Dec. 2017) in Assu-RN, Brazil (5°S, 37°W) (b), along with air mass (gray Xs) and precipitable water values (yellow triangles).

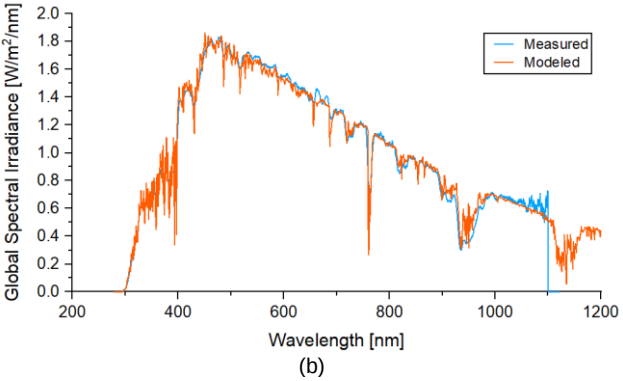
4.4 GIOVANNI + SMARTS METHOD: INSTANTANEOUS SPECTRUM

During field measurements, it is not always possible to have access to spectral measuring equipment, and historical spectral measured data are still scarce for many parts of the globe, Brazilian territory included. However, for atmospheric conditions such as those found in the Brazilian Northeast, where most PV plants are being deployed (Campos et al., 2018; Deschamps and Rüther, 2019), it has been shown that there is a significant spectral gain for both analyzed technologies (Figure 16), justifying the need for spectral correction of field measurements to standard test conditions (STC). To overcome the lack of spectral data, a spectral factor must be calculated directly from measured or historical environmental parameters (as shown in Section 3.6), or indirectly through the modeling of the local spectrum for the specific time and place in which a measurement was made, using locally measured or satellite-based environmental data (procedure explained in Section 3.6).

To evaluate the effectiveness of the proposed method for an instantaneous approximation of local spectrum, the method was tested for Florianópolis-SC during a clear day (Oct. 28th, 2017 at 12:00). Air mass value was obtained from NREL's solar position calculator (NREL, n.d.), while precipitable water, AOD, O_3 and CO_2 values were downloaded through the Giovanni platform using the same satellites mentioned in Table 4 . From the environmental data, an input file was generated using the metric shown in Table 5, and the pressure-corrected air mass for that instant.

The modeled and measured spectra are compared in Figure 17 for three distinct times of the day: (a) 9:00, time at which global tilted irradiance usually reaches minimum requirements for IV curve tracing (700 W/m² as local standard requires (ABNT, 2014)) in Florianópolis; (b) 12:00, time at which irradiance levels are close to their maximum; and (c) 15:00, around the time at which irradiance falls back below the minimum levels recommended for PV module measurements. For all three times chosen the comparison is very satisfactory proving that the SMARTS + Giovanni proposed method is considerably accurate for instantaneous spectral modeling for clear-days. Considering that PV system measurements are to be done under clear skies conditions, the method is well fitted for correction of field IV curve measurements.





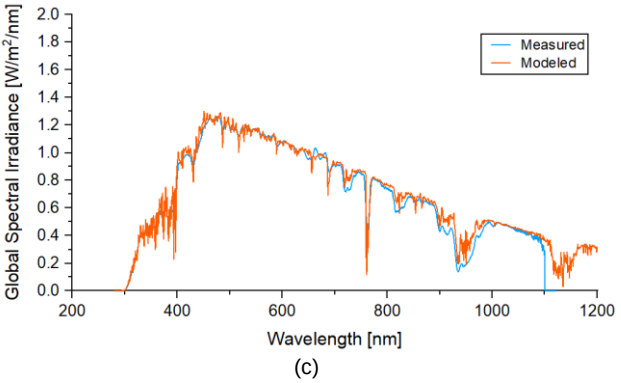


Figure 17 - Comparison between modeled spectrum (SMARTS + Giovanni method) and measured spectrum for Florianópolis-SC, Brazil (27°S, 48°W) at three distinct times of a clear-day (Oct. 28th, 2017): 9:00 (a); 12:00 (b); and 15:00 (c).

4.5 GIOVANNI + SMARTS METHOD: IRRADIANCE-WEIGHTED SPECTRUM

Another use for spectral correction is long-term data analysis. In the case of daily calculations for spectral impact on the PV system, a representative SF value for the day should be estimated. The first approach to find this representative value was calculating individual SF values for several moments of a clear day, and then filtering and averaging these values using an irradiance-weighted average. In order to apply this method, spectral measurements taken with a one-minute resolution were averaged for 15-minute intervals for a clear day (Oct. 28th, 2017) in Florianópolis-SC (spectra shown in Figure 18 (a)) and filtered for irradiances below 200 W/m^2 (irradiance profile shown in Figure 18 (b)). Consecutively, for each spectral measurement the SF for both mc-Si and new generation CdTe was calculated. From these values, two irradiance-weighted SF were obtained, one for each of the evaluated PV technologies. These results were then compared to the one obtained from first calculating an irradiance-weighted average spectrum for the day - also applying a 200 W/m^2 filter - and then calculating the SFs for mc-Si and CdTe. These results are compared in Table 7, and it can be seen that both approaches have reached the same results, meaning that an irradiance-weighted spectrum can be used to compute a representative spectral factor for a clear day.

Table 7 - Comparison between irradiance-weighted average SF and SF calculated from irradiance-weighted average spectrum for mc-Si and new generation CdTe for a clear day (Oct. 28th, 2017) in Florianópolis-SC, Brazil (27°S, 48°W).

PV Technology	Irradiance-weighted SF	SF calculated from irradiance-weighted spectrum
mc-Si	0.98	0.98
CdTe	1.01	1.01

Two paths could be followed to obtain this representative irradiance-weighted spectrum for the day using the Giovanni + SMARTS method proposed. The first approach would be modeling spectra for several instants of the day, and then calculating a daily irradiance-weighted spectrum. This would require several spectral simulations and several SF calculations, making this approach onerous.

Considering that the satellite databases used are in daily resolution (and so are most satellite-based sources), the only parameter variable throughout the day would be the air mass. This leads to a more straight-forward approach: calculate an irradiance-weighted air mass and use this value as an input to SMARTS - along with Giovanni-downloaded environmental parameters - to model a representative spectrum for the day. In this approach, air mass values for irradiances lower than 200 W/m^2 were filtered to avoid problems caused by large air mass values present in the beginning and end of the day. Figure 18 (a) presents the global horizontal irradiance (orange line) and air mass (gray Xs) profile for a clear day in Florianópolis-SC (Oct. 28th, 2017), as well as the 1.39 irradiance-filtered and weighted calculated AM (gray dashed line). For this specific day, irradiances below 200 W/m^2 represented only 2.5% of all the measured irradiation (energy).

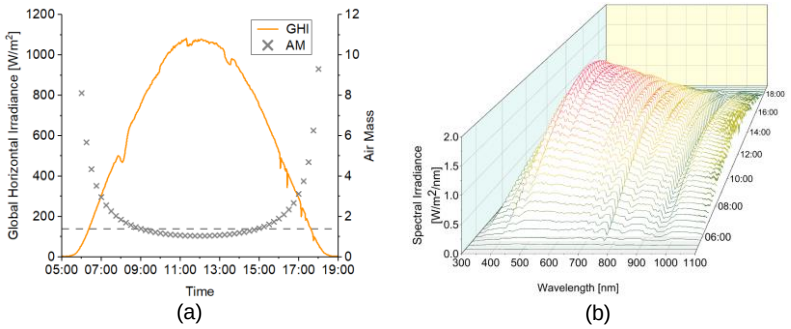


Figure 18 - Measured global horizontal irradiance (orange line), corresponding optical air mass (gray Xs) and irradiance-weighted air mass (gray dashed line) and (a), and solar spectral distribution with 15-minute-averaged resolution (b) for a clear-day (Oct. 28th, 2017) in Florianópolis-SC, Brazil (27°S, 48°W).

This approach to find the representative daily spectrum was applied to 28 non-consecutive days with diffuse fractions ranging from 10% up to 95% for Florianópolis-SC, between October 23rd and December 4th, 2017. Figure 19 shows the comparison between modeled and measured irradiance-weighted spectra for some of the days analyzed: (a) 10% diffuse fraction, 1.3 irradiance-weighted average AM; (b) 25%, AM1.2; (c) 38%, AM1.2; (d) 62%, AM1.4; (e) 71%, AM1.2; and (f) 91%, AM1.2. It can be seen that modeled spectra match measured spectra more closely for low-diffuse-fraction days, which was expected considering SMARTS is a model for clear skies.

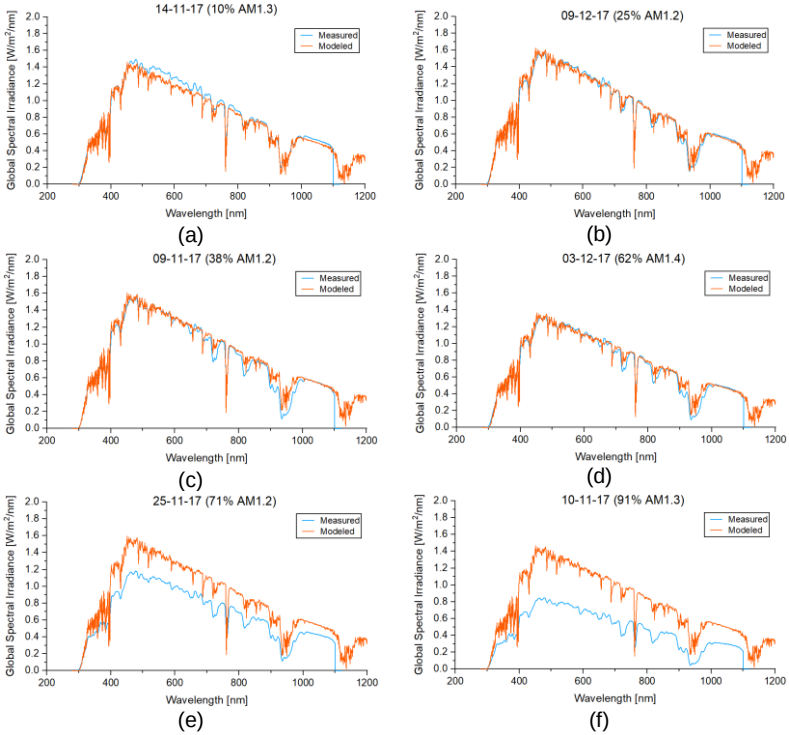


Figure 19 - Comparison between modeled (Giovanni + SMARTS method with irradiance-filtered and weighted AM, orange curve) and measured irradiance-weighted daily spectrum (blue curve) for several diffuse fractions in Florianópolis-SC, Brazil (27°S, 48°W).

The spectral factor was then calculated from modeled spectra for the above-mentioned days. These results were compared to the ones obtained from measured spectra. Figure 20 shows, for both mc-Si (red squares) and new generation CdTe (blue diamonds), the relative deviation between SF calculated from modeled and measured irradiance-filtered and weighted average spectra as a function of the daily diffuse fraction.

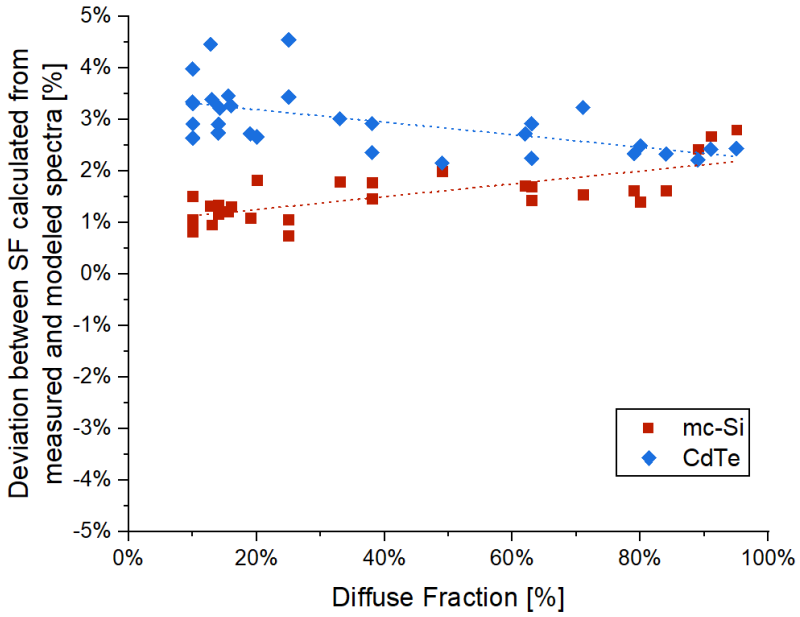


Figure 20 - Relative deviation between measured SF and SF computed from SMARTS modeled spectra using irradiance-filtered and weighted AM values for Florianópolis-SC, Brazil (27°S, 48°W) for mc-Si (red squares) and new generation CdTe (blue diamonds) as a function of diffuse fraction for the analyzed days.

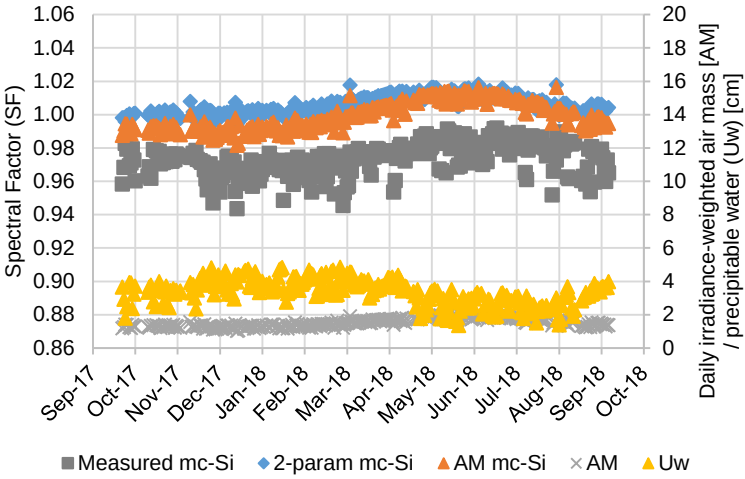
For mc-Si, deviation between SF calculated from modeled and measured spectra increases for days with higher diffuse fractions. This result was expected considering that SMARTS is a model for clear skies and cannot effectively model spectra for days with higher nebulosity. From Figure 19 it can be observed that days with higher diffuse fraction were over-estimated by the model, mainly within the 400 to 800 nm range, resulting in larger deviations for mc-Si. For new generation CdTe, the proposed method presented slightly better results for higher diffuse fractions than for clear days.

4.6 ASSESSMENT OF DIRECT METHODS FOR SF COMPUTATION

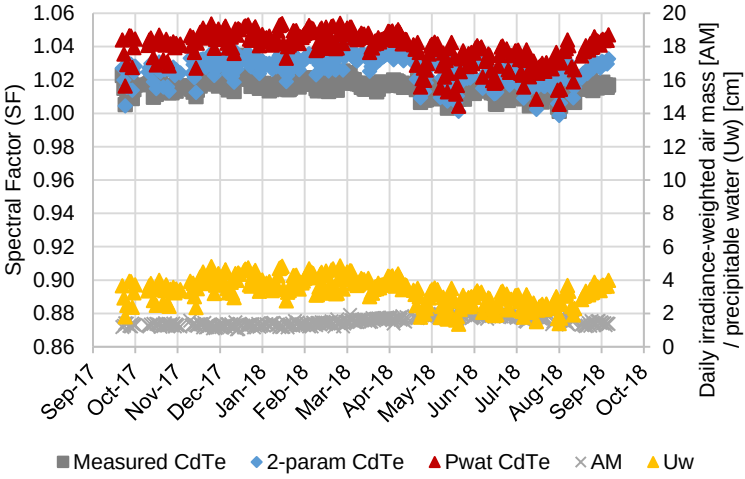
The three direct methods for the quantification of spectral impacts described in the prior section were applied to estimate the spectral impacts of the local environment on mc-Si and new generation CdTe for Florianópolis-SC. Locally measured environmental parameters - obtained from the solar monitoring station shown in Figure 9 and described in Table 2 with a one-minute time resolution from October 21st, 2017 through September 30th, 2018 - were used as inputs to the Sandia AM (for mc-Si), Pwat (for CdTe) and 2-parameter (mc-Si and CdTe) methods.

The estimated spectral factors were computed in the one-minute basis, then filtered for low irradiances (below 200 W/m^2) and daily irradiance-weighted averages were computed. The same was done for air mass and precipitable water values. The obtained results were then compared to spectral factors calculated from measured daily irradiance-filtered and weighted spectra for each individual day in the period analyzed. Only days with more than 500 minutes of valid data were accounted for. The daily results for mc-Si and new generation CdTe are shown in Figure 21 (a) and (b), respectively.

On Figure 21 (a), a seasonal variation can be observed for mc-Si, with this technology's SF presenting higher values around the Southern Hemisphere's winter solstice (June 21st), which can be explained by the lower altitude angle of the Sun's trajectory at that time, resulting in redder spectra for this time of the year. Also, Figure 21 (a) shows a lower precipitable water content for the winter months, also resulting in redder spectra. It can be observed that for the period close to the Southern Hemisphere's winter solstice (June 21st), the direct methods evaluated resulted in very similar spectral factors for mc-Si, showing that AM has a more significant impact on 2-parameter SF for mc-Si than precipitable water. Daily values of SF were averaged weighted by that day's irradiation, for measured data, the results obtained for mc-Si were as follow: 0.97 for measured spectra; 1.00 for Sandia's AM only method; and 1.01 for the 2-parameter method.



(a)



(b)

Figure 21 - SF results for measured spectra (gray squares) in comparison with 2-parameter method (blue diamonds, mc-Si and CdTe), Sandia's AM method (orange triangles, mc-Si only) and precipitable water method (red triangles, CdTe only), for mc-Si (a) and new generation CdTe (b) in Florianópolis-SC, Brazil (27°S, 48°W). Daily irradiance-filtered and weighted air mass (gray Xs) and precipitable water (yellow triangles) are also displayed on both graphs.

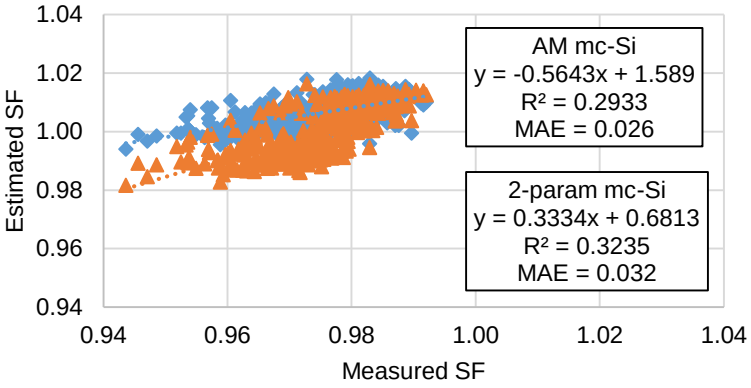
The opposite can be observed for new generation CdTe on Figure 21 (b), which presented lower spectral factors for the winter months, on account of this technology having a blue-biased response. There is also a slight reduction in the difference observed between SF estimated through the 2-parameter and the Pwat methods for the months near the winter solstice, implying that precipitable water has a greater impact on CdTe SF than AM, according to the 2-parameter method. The annual irradiation-weighted SF for new generation CdTe were: 1.02 for measured spectra; 1.04 for Pwat method; and 1.03 for the 2-parameter method. Figure 22 (a) and (b) present the correlation between measured SF and estimated SF for mc-Si and new generation CdTe, respectively.

For mc-Si, both AM and 2-parameter methods overestimated the local spectral impacts on the technology. On average, the AM method showed a 0.026 mean absolute error (MAE) when compared to SF calculated from measured spectra, while the 2-parameter method presented a 0.032 MAE. The direct methods also overestimated the spectral factor for CdTe, but the MAEs were only 0.024 and 0.011 for the Pwat and 2-parameter methods, respectively.

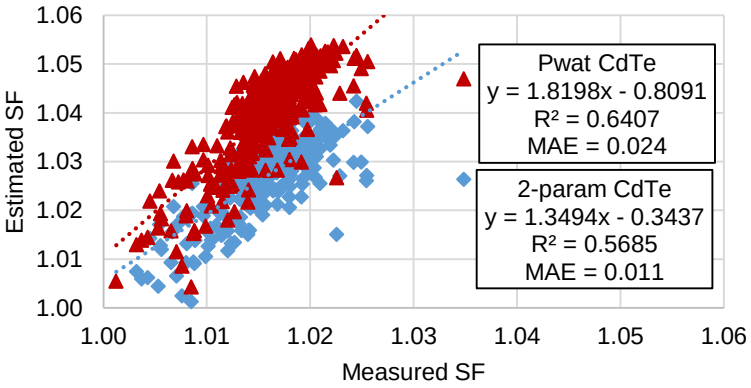
Figure 23 shows - for mc-Si (a) and new generation CdTe (b) - the deviation between estimated and measured SF for the three analyzed direct methods and the proposed method using data from the Giovanni platform, irradiance-filtered and weighted air mass and SMARTS spectra modeling for 28 non-consecutive days with diffuse fractions ranging from 10% up to 95% for Florianópolis-SC, between October 23rd and December 4th, 2017.

For mc-Si, all methods presented an increase in the difference between measured and estimated SF for days with higher diffuse fractions. The proposed Giovanni + SMARTS method demonstrated the best overall results for the 28 days evaluated, averaging a 0.014 absolute error. Sandia's AM method presented better results than the 2- parameter method - the opposite of what was previously found in the literature for the United States (Lee and Panchula, 2016) - with a 0.018 deviation versus 0.026 obtained from the 2-parameter method.

For CdTe, the direct methods did not show a dependence on diffuse fraction for the evaluated days. For this PV technology, the proposed Giovanni + SMARTS methodology averaged a 0.030 deviation from SF calculated from measured spectra, presenting slightly better results for days with higher diffuse fractions. The 2-parameter method performed the best, averaging a 0.009 deviation from measured SF, followed by the precipitable water only method, with a 0.025 deviation, results that corroborate previous findings from Lee and Panchula (2016).

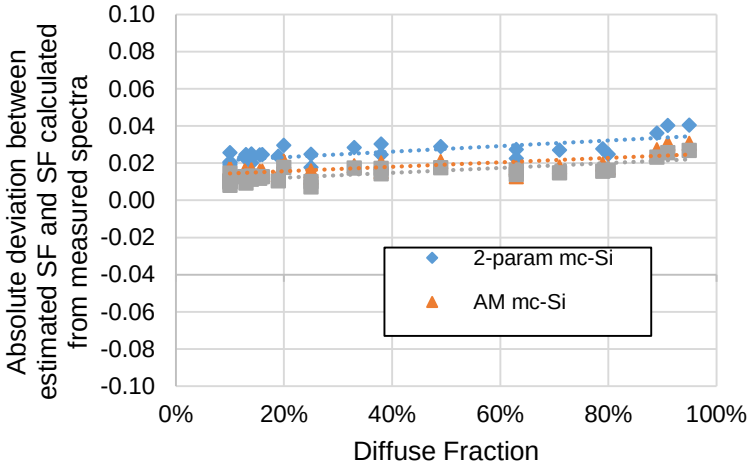


(a)

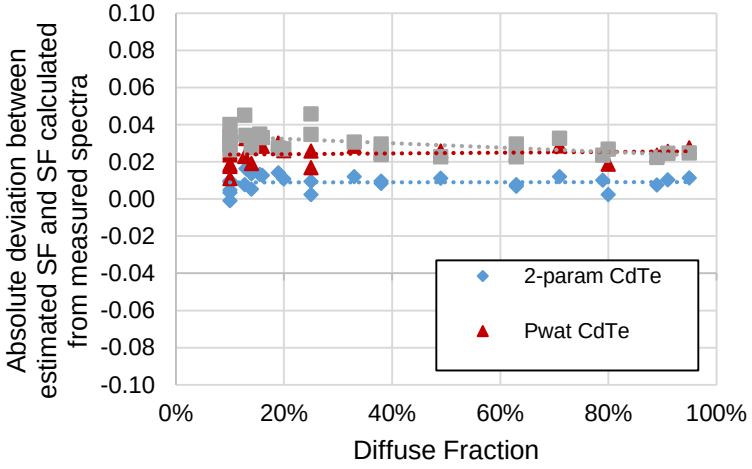


(b)

Figure 22 - Correlation between direct methods and measured SF for mc-Si (a) and new generation CdTe (b) for a full year of data from Florianópolis-SC, Brazil (27°S, 48°W). Sandia's AM method is shown as orange triangles (mc-Si only), Pwat method as red triangles (CdTe only) and the 2-parameter method as blue diamonds (mc-Si and CdTe).



(a)



(b)

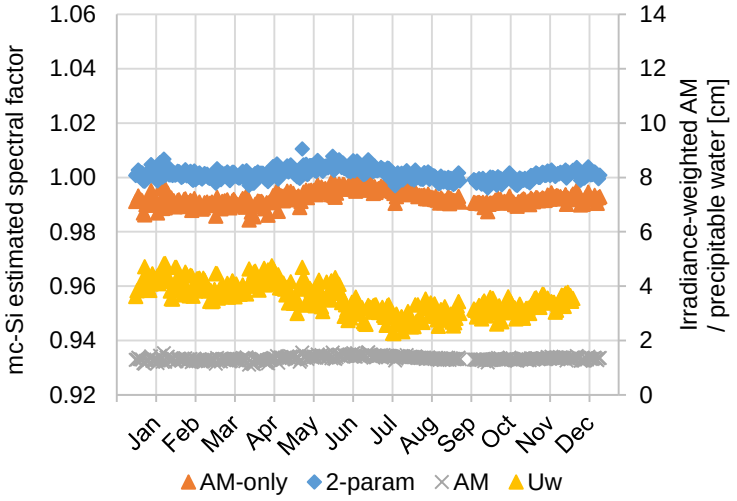
Figure 23 - Absolute deviation between SF calculated from measured spectra and SF estimated through Sandia's AM method (orange triangles, mc-Si only), Pwat method (red triangles, CdTe only), 2-parameter method (blue diamonds, mc-Si and CdTe) and the proposed Giovanni + SMARTS method (grays squares, mc-Si and CdTe) for mc-Si (a) and new generation CdTe (b) in Florianópolis-SC, Brazil (27°S, 48°W).

The three direct methods for the quantification of spectral impacts were also applied to estimate the spectral impacts of the local environment on mc-Si and new-generation CdTe at the Assu site. Locally measured environmental parameters were used as inputs to the AM-only (for mc-Si), Pwat-only (for CdTe) and 2-parameter (mc-Si and CdTe) methods. The estimated spectral factors were computed in the ten-minute basis, then filtered for low irradiances (< 200 W/m^2) and daily irradiance-weighted averages were calculated. The same was done for air mass (AM) and precipitable water (U_W) values. Only days with more than 500 minutes of valid data were accounted for. Daily results for mc-Si and new-generation CdTe are shown in Figure 24 (a) and (b), respectively.

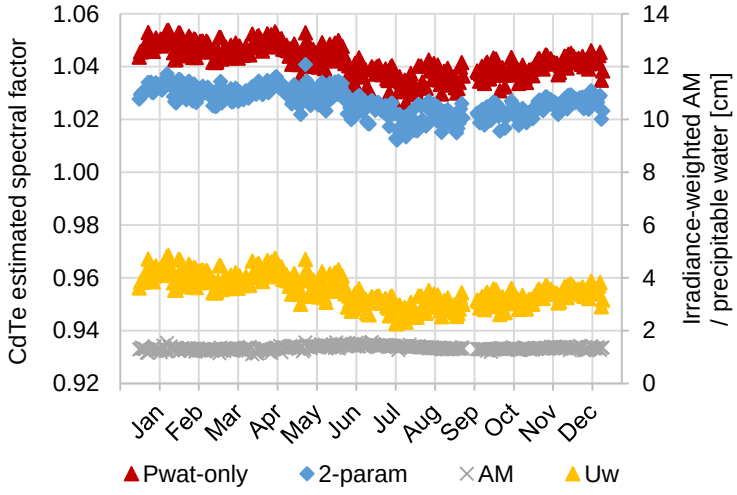
In Figure 24 (a), a seasonal variation can be observed for mc-Si, with this technology's spectral factor presenting higher values around the Southern Hemisphere's winter solstice (Jun 21st), when irradiance-weighted AM values are also higher, resulting in redder spectra for this time of the year. Additionally, Figure 24 (a) shows a lower precipitable water content for the winter months. Daily values of spectral factor were averaged-weighted by that day's irradiation, the results for mc-Si were 0.99 for AM-only and 1.00 for the 2-parameter method. For the AM-only method, the spectral factor values ranged from 0.98 to 1.00 and for 2-parameter from 1.00 to 1.01.

The opposite seasonal variation can be observed for new-generation CdTe in Figure 24 (b), which presented lower spectral factors for the winter months, on account of this technology having a blue-biased spectral response. There is also a slight reduction in the difference observed between SF estimated through the 2-parameter and the Pwat methods for the months near the winter solstice. Implying that precipitable water has a greater impact on CdTe SF than AM, according to the 2-parameter method. The annual irradiation-weighted spectral factor for new-generation CdTe were 1.04 for Pwat-only and 1.03 for the 2-parameter method. Daily spectral factor values ranged from 1.02 to 1.05 for Pwat-only and from 1.01 to 1.04 for 2-parameter method.

A summary of results for annual evaluation of direct methods for the Assu-RN site with minimum and maximum daily values, as well as annual irradiation-weighted averages are shown in Table 8.



(a)



(b)

Figure 24 - Daily average air mass (gray Xs), precipitable water (yellow triangles) and spectral factor estimated from measured data for Assu-RN, Brazil (5°S, 37°W) using the 2-parameter (blue diamonds), AM-only (orange triangles) and Pwat-only (red triangles) methods, for mc-Si (a) and new-generation CdTe (b).

Table 8 - Minimum and maximum daily irradiance-weighted and filtered averages, and annual irradiation-weighted averages for SF and measured environmental parameter for the Assu-RN, Brazil (5°S, 37°W) site.

PV Technology	***Method***	***Daily Min.***	***Daily Max.***	***Annual Avg.***
mc-Si	AM-only	0.98	1.00	0.99
mc-Si	2-param	1.00	1.01	1.00
CdTe	Pwat	1.02	1.05	1.04
CdTe	2-param	1.01	1.04	1.03
Air Mass (AM)		1.11	1.57	1.35
Precipitable Water (U_w)		2.26 cm	4.84 cm	3.49 cm
Global Horizontal Irradiation (GHI)		1.77 W/m^2	7.60 W/m^2	5.66 W/m^2
Ambient Temperature (T_{amb})		26.99°C	34.80°C	32.53°C

The performance of the direct methods evaluated in this study corroborate previous findings from Lee and Panchula (2016) for new generation CdTe in establishing which methods performed better; however, for the mentioned study, the authors have found the direct methods to underestimate the spectral factor, whereas here the opposite was observed for Florianópolis. This might be due to the fact that these methods are empirical approximations computed from data measured in the United States, and would be expected to respond differently to the blue-bias Brazilian spectral distribution of sunlight.

5 PRELIMINARY CONCLUSIONS

This thesis aims at evaluating alternatives for the calculation of spectral factors for long-term data analysis and for instantaneous measurement corrections. Long-term spectral impacts must be evaluated in the analysis of historical and current performance data of existing PV systems and in the energy yield estimation of future systems, especially for utility-scale power plants market which is expanding rapidly all over the world. For field evaluations, instantaneous spectral correction is necessary for the correction of measured peak-power values to STC conditions, especially during the commissioning of utility-scale power plants.

Firstly, the impacts of environmental variables were assessed through the SMARTS modeling of the standard ASTM G173-03 spectrum varying one parameter at a time. The results showed that air mass has the greatest impact on spectra, especially within the visible light range (400-750 nm), when AM varied from 1.0 to 6.0. Increasing AOD values also resulted in the attenuation of spectral content on shorter wavelengths (500 - 700 nm). Spectral factors calculated for mc-Si and new generation CdTe showed that larger AM and AOD values (meaning redder spectra) have a positive impact on mc-Si and a negative impact on new generation CdTe, due to its narrow blue-shifted spectral response. Higher precipitable water values led to spectral gains for CdTe, since it attenuates longer wavelengths (950-1150 nm), outside of this technology's spectral response range. Ozone values ranged from 0.00 to 0.50 atm-cm in this analysis, and the results showed a minor attenuation in the spectral distribution within 500 and 700 nm. Carbon dioxide was varied from 200 to 600 ppmv and showed no significant impacts on the distribution of modeled spectra. The results from this part of the study agree with similar analyses performed by Betts (2004), Haag (2012), Litjens (2013), Stark and Theristis (2015) and Lee and Panchula (2016).

The spectral impacts of measured spectra from two distinct locations in Brazil (Florianópolis, in the South and Assu, in the Northeast) were evaluated for mc-Si and new generation CdTe. It was shown that both locations presented great spectral advantages for new generation CdTe, with spectral gains up to 2% for irradiance levels above 200 W/m^2 for Florianópolis and and impressive 10% for Assu. The spectral gains for new generation CdTe at these sites can be attributed to the small relative optical air mass found in low-latitude regions and to the high precipitable water content present at the sites when compared to the reference spectrum (2.43 cm for Florianópolis and 3.42 cm for Assu,

compared to 1.416 cm of ASTM G173-03). The irradiance-filtered and weighted SF for new generation CdTe calculated for Assu during the evaluated period (between November 21st and December 15th, 2017) was 1.09, and 1.01 for Florianópolis on October 28th, 2017 (SF values for irradiances below 200 W/m^2 were disregarded).

Multicrystalline silicon presented spectral factors that ranged from 0.98 to 1.00 for irradiance levels above 200 W/m^2 for Florianópolis, reaching SF values above 1 (representing gains) only for early morning and late afternoon (air mass values above 3, meaning redder spectra), and the irradiance-filtered and weighted average obtained for this technology was 0.98. The lower SF for mc-Si can be attributed to the blue-shifted spectral distribution of the region, caused by high precipitable water content and overall low relative optical air mass values. For Assu, a strong correlation between air mass and SF for both technologies could be observed. For air mass values greater than 2 there is an abrupt increase in SF for mc-Si, corroborating the results obtained from modeled reference spectra with varying air mass. SF values for mc-Si ranged from 1.00 to 1.06 during the evaluated period, with an irradiance-filtered and weighted average of 1.02.

The proposed methodology employing Giovanni downloaded data and the SMARTS model was also tested as a method for correction of field instantaneous measurements. The results for modeled vs. measured spectra were satisfactory for all three evaluated times of the day (9:00, 12:00 and 15:00, times during which minimum irradiance levels are met, allowing field measurements at the specific site), showing that the use of satellite data as inputs to the SMARTS model is a good approach to model spectra for clear skies conditions, which are the expected conditions for field measurements.

Overall, the proposed method using satellite data from NASA's Giovanni platform along with air mass and SMARTS model yielded good results for both long-term and instantaneous spectral impact evaluation. Further work must be carried out to simplify the computation process and expedite the calculations, making it possible for the method to be applied to a larger set of data. Also, it is important to highlight that a quantitative uncertainty analysis is recommended in order to better evaluate results obtained through the proposed methodology.

6 WORKPLAN AND TIMELINE

		2019									2020											
		May	Jun	Jul	Aug	Sep	Oct	Nov	Dec		Jan	Feb	Mar	Apr	May	Jun	Jul	Aug	Sep	Oct	Nov	Dec
Local Spectrum Characterization	*Development of methods for spectral data treatment*																					
	Development of a numerical model for spectral impact calculation																					
	Analysis of measured spectra																					
Validation of SMARTS model for Brazil	*Spectral modeling from satellite data*																					
	Comparison with measured spectra																					
	Results analysis																					
Direct Methods Evaluation	*Development of a spreadsheet to calculate spectral factors using the direct methods*																					
	Calculate spectral impact using satellite and locally measured data																					
	Evaluation of new coefficients to better fit methods to the Brazilian climate																					
	Testing of new coefficients using direct methods vs. measured spectral factors																					
Brazilian Spectral Impact Map	*Choose site to evaluate spectral impacts*																					
	Download satellite data for the chosen sites																					
	Spactra modeling using SMARTS																					
	Evaluation of spectral impacts for the chosen sites using modeled spectra and direct methods																					
	Mapping out spectral impacts for mc-Si and CdTe throughout Brazil																					
	Evaluate seasonality of spectral effects on the chosen sites																					
Measurements and Literature Review	*Continuos spectral, weather and satellite data collection*																					
	Extensive literature review																					
	Writing thesis																					
	Articles writing and submission*																					
	Final presentation																					

		2021												2022												2023		
		Jan	Feb	Mar	Apr	May	Jun	Jul	Aug	Sep	Oct	Nov	Dec	Jan	Feb	Mar	Apr	May	Jun	Jul	Aug	Sep	Oct	Nov	Dec	Jan	Feb	Mar
Local Spectrum Characterization	*Development of methods for spectral data treatment*																											
	Development of a numerical model for spectral impact calculation																											
	Analysis of measured spectra																											
Validation of SMARTS model for Brazil	*Spectral modeling from satellite data*																											
	Comparison with measured spectra																											
	Results analysis																											
Direct Methods Evaluation	*Development of a spreadsheet to calculate spectral factors using the direct methods*																											
	Calculate spectral impact using satellite and locally measured data																											
	Evaluation of new coefficients to better fit methods to the Brazilian climate																											
	Testing of new coefficients using direct methods vs. measured spectral factors																											
Brazilian Spectral Impact Map	*Choose site to evaluate spectral impacts*																											
	Download satellite data for the chosen sites																											
	Spactra modeling using SMARTS																											
	Evaluation of spectral impacts for the chosen sites using modeled spectra and direct methods																											
	Mapping out spectral impacts for mc-Si and CdTe throughout Brazil																											
	Evaluate seasonality of spectral effects on the chosen sites																											
Measurements and Literature Review	*Continuos spectral, weather and satellite data collection*																											
	Extensive literature review																											
	Writing thesis																											
	Articles writing and submission*																											
	Final presentation																											

*First article submitted on March 23rd, 2019 to Solar Energy, accepted with minor reviews on May 23rd, 2019.

REFERENCES

ABNT, 2014. NBR 16274: Sistemas fotovoltaicos conectados a rede - Requisitos mínimos para documentação, ensaios de comissionamento, inspeção e avaliação de desempenho.

ABNT, 2006. NBR 10899:2006 - Energia Solar Fotovoltaica - Terminologia.

Alvares, C.A., Stape, J.L., Sentelhas, P.C., De Moraes Gonçalves, J.L., Sparovek, G., 2013. Köppen's climate classification map for Brazil. Meteorol. Zeitschrift 22, 711–728. https://doi.org/10.1127/0941-2948/2013/0507

Amillo, A.M.G., Huld, T., Vourlioti, P., Müller, R., Norton, M., 2015. Application of satellite-based spectrally-resolved solar radiation data to PV performance studies. Energies 8, 3455–3488. https://doi.org/10.3390/en8053455

ASTM, 2012. G173-03 Standard Tables for Reference Solar Spectral Irradiances : Direct Normal and Hemispherical on 37° Tilted Surface. Am. Soc. Test. Mater. https://doi.org/10.1520/G0173-03R12

Betts, T.R., 2004. Investigation of photovoltaic device operation under varying spactral conditions. Loughborough University.

Bird, R.E., Hulstrom, R.L., Lewis, L.J., 1983. Terrestrial solar spectral data sets. Sol. Energy 30, 563–573. https://doi.org/10.1016/0038-092X(83)90068-3

Bolinger, M., Weaver, S., Zuboy, J., 2015. Is $50/MWh solar for real? Falling project prices and rising capacity factors drive utility-scale PV toward economic competitiveness. Prog. Photovoltaics Res. Appl. 23, 1847–1856. https://doi.org/10.1002/pip.2630

Bosio, A., Rosa, G., Romeo, N., 2018. Past, present and future of the thin film CdTe/CdS solar cells. Sol. Energy 175, 31–43. https://doi.org/10.1016/j.solener.2018.01.018

Burger, B., Rüther, R., 2006. Inverter sizing of grid-connected photovoltaic systems in the light of local solar resource distribution characteristics and temperature. Sol. Energy 80, 32–45. https://doi.org/10.1016/j.solener.2005.08.012

Campos, R.A., Nascimento, L.R. do, Braga, M., Simoes, G., Ruther, R., 2018. Performance Assessment of PV Technologies and Complementarity of Utility-Scale PV and Wind Power Plants in Brazil, in: 2018 IEEE 7th World Conference on Photovoltaic Energy Conversion (WCPEC) (A Joint Conference of 45th IEEE PVSC, 28th PVSEC & 34th EU PVSEC). IEEE, pp. 1173–1178. https://doi.org/10.1109/PVSC.2018.8547259

Dash, P.K., Gupta, N.C., Rawat, R., Pant, P.C., 2017. A novel climate classification criterion based on the performance of solar photovoltaic technologies. Sol. Energy 144, 392–398.

https://doi.org/10.1016/j.solener.2017.01.046
Deschamps, E.M., Rüther, R., 2019. Optimization of Inverter Loading Ratio for Grid Connected Photovoltaic Systems. Sol. Energy 179, 106–118. https://doi.org/J.SOLENER.2018.12.051
Dirnberger, D., Blackburn, G., Müller, B., Reise, C., 2015a. On the impact of solar spectral irradiance on the yield of different PV technologies. Sol. Energy Mater. Sol. Cells 132, 431–442. https://doi.org/10.1016/j.solmat.2014.09.034
Dirnberger, D., Müller, B., Reise, C., 2015b. PV module energy rating: opportunities and limitations. Prog. Photovoltaics Res. Appl. 23, 1754–1770. https://doi.org/10.1002/pip.2618
Dirnberger, D., Müller, B., Reise, C., 2015c. On the uncertainty of energetic impact on the yield of different PV technologies due to varying spectral irradiance. Sol. Energy. https://doi.org/10.1016/j.solener.2014.10.033
Dirnberger, D., Reise, C., 2015. On the uncertainty of energetic impact on the yield of different PV technologies due to varying spectral irradiance. Sol. Energy 111, 82–96. https://doi.org/10.1016/j.solener.2014.10.033
Dornelles, K.A., Roriz, M., Roriz, V.F., Caram, R.M., 2015. Thermal performance of white solar-reflective paints for cool roofs and the influence on the thermal comfort and building energy use in hot climates 3. https://doi.org/10.13140/RG.2.1.1745.5843
Duck, B.C., Fell, C.J., 2015. Comparison of methods for estimating the impact of spectrum on PV output, in: 2015 IEEE 42nd Photovoltaic Specialist Conference, PVSC 2015. IEEE, pp. 1–6. https://doi.org/10.1109/PVSC.2015.7356211
Eltbaakh, Y.A., Ruslan, M.H., Alghoul, M.A., Othman, M.Y., Sopian, K., Razykov, T.M., 2012. Solar attenuation by aerosols: An overview. Renew. Sustain. Energy Rev. 16, 4264–4276. https://doi.org/10.1016/j.rser.2012.03.053
EPE, 2017. EPE-DEE-RE-065/2013-R4: Instruções para Solicitação de Cadastramento e Habilitação Técnica com vistas à participação nos Leilões de Energia Elétrica.
Fernandez, E.F., Cruz, F.A., Mallick, T.K., Sundaram, S., 2015. Effect of Spectral Irradiance Variations on the Performance of Highly Efficient Environment-Friendly Solar Cells. IEEE J. Photovoltaics 5, 1150–1157. https://doi.org/10.1109/JPHOTOV.2015.2434593
Fernández, E.F., Soria-Moya, A., Almonacid, F., Aguilera, J., 2016. Comparative assessment of the spectral impact on the energy yield of high concentrator and conventional photovoltaic technology. Sol. Energy Mater. Sol. Cells 147, 185–197. https://doi.org/10.1016/j.solmat.2015.12.003
Field, H., Emery, K., 1993. An uncertainty analysis of the spectral correction factor, in: 23rd IEEE Photovoltaic Specialists Conference. pp. 1180–

1187. https://doi.org/10.1109/PVSC.1993.346955
First Solar, 2018a. First Solar Series 6TM Thin Film Modules - Next Generation Solar Energy.
First Solar, 2018b. PD-5-401-06: First Solar Series 6TM Module Datasheet.
First Solar, 2017. PD-5-445 Rev 1.0: Module Characterization - Spectral Response of FS Series PV Modules.
First Solar, n.d. PlantPredict [WWW Document]. URL https://plantpredict.com/algorithm/optical-losses/#precipitable-water-method (accessed 11.13.18).
Fraunhofer Institute for Solar Energy Systems, 2019. Photovoltaics Report.
Fraunhofer Institute for Solar Energy Systems, 2011. Photovoltaics Report.
Gottschalg, R., Betts, T.R., Infield, D.G., Kearney, M.J., 2005. The effect of spectral variations on the performance parameters of single and double junction amorphous silicon solar cells. Sol. Energy Mater. Sol. Cells 85, 415–428. https://doi.org/10.1016/j.solmat.2004.05.011
Gottschalg, R, Infield, D.G., Kearney, M.J., 2003. Experimental study of variations of the solar spectrum of relevance to thin film solar cells. Sol. Energy Mater. Sol. Cells 79, 527–537. https://doi.org/10.1016/S0927-0248(03)00106-5
Gottschalg, R., Infield, D.G., Kearney, M.J., 2003. Experimental study of variations of the solar spectrum of relevance to thin film solar cells. Sol. Energy Mater. Sol. Cells 79, 527–537. https://doi.org/10.1016/S0927-0248(03)00106-5
Green, M.A., Emery, K., Hishikawa, Y., Warta, W., Dunlop, E.D., 2016. Solar cell efficiency tables (version 48). Prog. Photovolt Res. Appl. 24, 905–913. https://doi.org/10.1002/pip
Green, M.A., Emery, K., Hishikawa, Y., Warta, W., Dunlop, E.D., 2015. Solar cell efficiency tables (version 46). Prog. Photovolt Res. Appl. 23, 805–812. https://doi.org/10.1002/pip.2637
Green, M.A., Hishikawa, Y., Dunlop, E.D., Levi, D.H., Hohl-Ebinger, J., Yoshita, M., Ho-Baillie, A.W.Y., 2019. Solar cell efficiency tables (Version 53). Prog. Photovoltaics Res. Appl. 27, 3–12. https://doi.org/10.1002/pip.3102
Gueymard, C., 2006. SMARTS code (version 2.9.5). User's manual 50.
Gueymard, C., 1995. A Simple Model of the Atmospheric Radiative Transfer of Sunshine: Algorithms and performance assessment. Florida Sol. Energy Cent.
Gueymard, C., 1994. Analysis of monthly average atmospheric precipitable water and turbidity in Canada and Northern United States. Sol. Energy 53, 57–71. https://doi.org/10.1016/S0038-092X(94)90606-8
Gueymard, C.A., 2014. Impact of on-site atmospheric water vapor estimation methods on the accuracy of local solar irradiance predictions. Sol. Energy 101, 74–82. https://doi.org/10.1016/j.solener.2013.12.027

Gueymard, C.A., 2003. Direct solar transmittance and irradiance predictions with broadband models. Part I: detailed theoretical performance assessment. Sol. Energy 74, 355–379. https://doi.org/10.1016/S0038-092X(03)00195-6

Gueymard, C.A., Myers, D., Emery, K., 2002. Proposed reference irradiance spectra for solar energy systems testing. Sol. Energy 73, 443–467. https://doi.org/10.1016/S0038-092X(03)00005-7

Haag, R., 2012. Estimativa da distribuição espectral da radiação solar sobre o território brasileiro através de análise multiinstrumental.

Haag, R., Krenzinger, A., 2016. Espectro solar característico para a região do semiárido brasileiro, in: VI Congresso Brasileiro de Energia Solar.

Hohl-Ebinger, J., Warta, W., 2011. Uncertainty of the spectral mismatch correction factor in STC measurements on photovoltaic devices. Prog. Photovoltaics Res. Appl. https://doi.org/10.1002/pip.1059

Huld, T., Dunlop, E., Beyer, H.G., Gottschalg, R., 2013. Data sets for energy rating of photovoltaic modules. Sol. Energy 93, 267–279. https://doi.org/10.1016/j.solener.2013.04.014

Huld, T., Gracia Amillo, A.M., 2015. Estimating PV module performance over large geographical regions: The role of irradiance, air temperature, wind speed and solar spectrum. Energies 8, 5159–5181. https://doi.org/10.3390/en8065159

Hulstrom, R., Bird, R., Riordan, C., 1985. Spectral solar irradiance data sets for selected terrestrial conditions. Sol. Cells 15, 365–391. https://doi.org/10.1016/0379-6787(85)90052-3

International Electrotechnical Commission, 2009. IEC 60891 Photovoltaic devices - Procedures for temperature and irradiance corrections to measured I-V characteristics.

International Electrotechnical Commission, 2008. IEC 60904-7 Photovoltaic devices - Part 7: Computation of the spectral mismatch correction for measurements of photovoltaic devices.

Jardine, C.N., Betts, T.R., Gottschalg, R., Infield, D.G., Lane, K., 2002. Influence of Spectral Effects on the Performance of Multijunction Amorphous, in: Proceedings of The17th European Photovoltaic Solar Energy Conference. München, Germany, pp. 2–5.

Kavlak, G., McNerney, J., Trancik, J.E., 2018. Evaluating the causes of cost reduction in photovoltaic modules. Energy Policy 123, 700–710. https://doi.org/10.1016/j.enpol.2018.08.015

King, B.H., Hansen, C.W., Riley, D., Robinson, C.D., Pratt, L., 2016. Procedure to Determine Coefficients for the Sandia Array Performance Model (SAPM).

King, D.L., Boyson, W.E., Kratochvil, J.A., 2002. Analysis of factors influencing the annual energy production of photovoltaic systems, in: 29th IEEE Photovoltaic Specialists Conference. IEEE, New Orle, pp.

1356–1361. https://doi.org/10.1109/PVSC.2002.1190861
King, D.L., Boyson, W.E., Kratochvill, J.A., 2004. Photovoltaic Array Performance Model (SAND2004-3535).
King, D.L., Eckert, P.E., 1996. Characterizing (rating) the performance of large photovoltaic arrays for all operating conditions. Conf. Rec. Twenty Fifth IEEE Photovolt. Spec. Conf. 1385–1388. https://doi.org/10.1109/PVSC.1996.564391
King, D.L., Kratochvil, J.A., Boyson, W.E., 1997. Measuring solar spectral and angle-of-incidence effects on photovoltaic modules and solar irradiance sensors, in: 26th IEEE Photovoltaic Specialists Conference. Anaheim, CA, pp. 1113–1116. https://doi.org/10.1109/PVSC.1997.654283
Kinsey, G.S., 2015. Spectrum sensitivity, energy yield, and revenue prediction of PV modules. IEEE J. Photovoltaics 5, 258–262. https://doi.org/10.1109/JPHOTOV.2014.2370256
Lad, R., Wohlgemuth, J., TamizhMani, G., 2010. Outdoor energy ratings and spectral effects of photovoltaic modules, in: 35th IEEE Photovoltaic Specialists Conference. IEEE, pp. 002827–002832. https://doi.org/10.1109/PVSC.2010.5616859
Lee, M., Ngan, L., Hayes, W., Panchula, A.F., 2015a. Comparison of the effects of spectrum on cadmium telluride and monocrystalline silicon photovoltaic module performance, in: 42nd Photovoltaic Specialist Conference. IEEE, pp. 1–4. https://doi.org/10.1109/PVSC.2015.7356174
Lee, M., Ngan, L., Hayes, W., Sorensen, J., Panchula, A.F., 2015b. Understanding next generation cadmium telluride photovoltaic performance due to spectrum. 42nd Photovolt. Spec. Conf. 1–6. https://doi.org/10.1109/PVSC.2015.7356003
Lee, M., Panchula, A., 2016. Spectral correction for photovoltaic module performance based on air mass and precipitable water. 43rd Photovolt. Spec. Conf. 1351–1356. https://doi.org/10.1109/PVSC.2016.7749836
Litjens, G., 2013. Investigation of Spectral Effects on Photovoltaic Technologies by Modelling the Solar Spectral Distribution. Universiteit Utrecht.
Minnaert, B., Veelaert, P., 2014. A proposal for typical artificial light sources for the characterization of indoor photovoltaic applications. Energies 7, 1500–1516. https://doi.org/10.3390/en7031500
Mints, P., 2018. SPV Market Solar Flare Report 2018 - Issue 3.
Munshi, A.H., Sasidharan, N., Pinkayan, S., Barth, K.L., Sampath, W.S., Ongsakul, W., 2018. Thin-film CdTe photovoltaics – The technology for utility scale sustainable energy generation. Sol. Energy 173, 511–516. https://doi.org/10.1016/j.solener.2018.07.090
Myers, D.R., Emery, K., Gueymard, C., 2002. Terrestrial solar spectral

modeling tools and applications for photovoltaic devices, in: 29th IEEE Photovoltaic Specialists Conference. IEEE, New Orleans, pp. 1683–1686. https://doi.org/10.1109/PVSC.2002.1190943

Myers, D.R., Gueymard, C. a, 2004. Description and Availability of the SMARTS Spectral Model for Photovoltaic Applications. NREL 1–12. https://doi.org/10.1117/12.555943

Nann, S., Emery, K., 1992. Spectral effects on PV-device rating. Sol. Energy Mater. Sol. Cells 27, 189–216. https://doi.org/10.1016/0927-0248(92)90083-2

NASA, n.d. NASA Giovanni [WWW Document]. URL https://giovanni.gsfc.nasa.gov/giovanni/

Nelson, L., Frichtl, M., Panchula, A., 2013. Changes in cadmium telluride photovoltaic system performance due to spectrum. IEEE J. Photovoltaics 3, 488–493. https://doi.org/10.1109/JPHOTOV.2012.2226868

NREL, 2018. Best Research-Cell Efficiencies [WWW Document]. URL https://www.nrel.gov/pv/assets/pdfs/pv-efficiencies-07-17-2018.pdf (accessed 12.5.18).

NREL, n.d. MIDC SOLPOS Calculator [WWW Document]. URL https://midcdmz.nrel.gov/solpos/solpos.html (accessed 11.19.18).

Núñez, R., Jin, C., Victoria, M., Domínguez, C., Askins, S., Herrero, R., Antón, I., Sala, G., 2016. Spectral study and classification of worldwide locations considering several multijunction solar cell technologies. Prog. Photovoltaics Res. Appl. 24, 1214–1228. https://doi.org/10.1002/pip.2781

Parida, B., Iniyan, S., Goic, R., 2011. A review of solar photovoltaic technologies. Renew. Sustain. Energy Rev. 15, 1625–1636. https://doi.org/10.1016/j.rser.2010.11.032

Parkinson, G., 2017. Chile solar auction sets new record low for solar PV [WWW Document]. RENEW Econ. URL https://reneweconomy.com.au/chile-solar-auction-sets-new-record-low-for-solar-pv-85114/ (accessed 12.5.18).

Parkinson, G., 2016. Solar price hits record low of 2.42c/kWh, and may fall further [WWW Document]. RENEW Econ. URL https://reneweconomy.com.au/solar-price-hits-record-low-of-2-42ckwh-and-may-fall-further-32358/ (accessed 12.5.18).

Peel, M.C., Finlayson, B.L., McMahon, T.A., 2007. Updated world map of the Köppen-Geiger climate classification. Hydrol. Earth Syst. Sci. 11, 1633–1644. https://doi.org/10.5194/hess-11-1633-2007

Perry, M., Troccoli, A., 2015. Impact of a fire burn on solar irradiance and PV power. Sol. Energy 114, 167–173. https://doi.org/10.1016/j.solener.2015.01.005

Reich, N.H., Mueller, B., Armsbruster, A., van Sark, W.G.J.H.M., Kiefer, K.,

Reise, C., 2012. Performance ratio revisited: is PR>90% realistic? Prog. Photovolt Res. Appl. 20, 717–726. https://doi.org/10.1002/pip.1219

Rodrigo, P.M., Fernández, E.F., Almonacid, F.M., Pérez-Higueras, P.J., 2017. Quantification of the spectral coupling of atmosphere and photovoltaic system performance: Indexes, methods and impact on energy harvesting. Sol. Energy Mater. Sol. Cells 163, 73–90. https://doi.org/10.1016/j.solmat.2017.01.018

Roy, J., Bliss, M., Betts, T.R., Gottschalg, R., 2010. Effect of I-V translations of irradiance-temperature on the energy yield prediction of PV module and spectral changes over irradiance and temperature, in: C92 Proceedings of the 6th Photovoltaic Science Applications and Technology Conference (PVSAT-6). pp. 149–152.

Rüther, R., 2004. Edifícios solares fotovoltaicos: o potencial da geração solar fotovoltaica integrada a edificações urbanas e interligada à rede elétrica pública no Brasil, UFSC-LABSOLAR.

Rüther, R., Kleiss, G., Reiche, K., 2002. Spectral effects on amorphous silicon solar module fill factors. Sol. Energy Mater. Sol. Cells 71, 375–385. https://doi.org/10.1016/S0927-0248(01)00095-2

Rüther, R., Livingstone, J., 1994. Seasonal variations in amorphous silicon solar module outputs and thin film characteristics. Sol. Energy Mater. Sol. Cells 36, 29–43. https://doi.org/10.1016/0927-0248(94)00165-O

Saga, T., 2010. Advances in crystalline silicon solar cell technology for industrial mass production. NPG Asia Mater. 2, 96–102. https://doi.org/10.1038/asiamat.2010.82

Senthilarasu, S., Fernández, E.F., Almonacid, F., Mallick, T.K., 2015. Effects of spectral coupling on perovskite solar cells under diverse climatic conditions. Sol. Energy Mater. Sol. Cells 133, 92–98. https://doi.org/10.1016/j.solmat.2014.10.037

Stark, C., Theristis, M., 2015. The impact of atmospheric parameters on the spectral performance of multiple photovoltaic technologies. 2015 IEEE 42nd Photovolt. Spec. Conf. PVSC 2015. https://doi.org/10.1109/PVSC.2015.7355836

Strevel, N., 2017. The Optimal PV Module Size.

Sutterlueti, J., Ransome, S., Kravets, R., Schreier, L., 2008. Characterising PV modules under outdoor conditions: what´s most important for energy yield, in: Proceedings of the 26th European Photovoltaic Solar Energy Conference and Exhibition. Hamburg, Germany.

Tsuji, M., Rahman, M.M., Hishikawa, Y., Nishioka, K., Minemoto, T., 2018. Uniqueness verification of solar spectrum obtained from three sites in Japan based on similar index of average photon energy. Sol. Energy 173, 89–96. https://doi.org/10.1016/j.solener.2018.07.039

Williams, S.R., Betts, T.R., Helf, T., Gottschalg, R., Beyer, H.G., Infield,

D.G., 2003. Modelling long-term module performance based on realistic reporting conditions with consideration to spectral effect, in: Proceedings of the 3rd World Conference on Photovoltaic Energy Conversion. Osaka, Japan, pp. 3–6.

Ye, J.Y., Reindl, T., Aberle, A.G., Walsh, T.M., 2014. Effect of Solar Spectrum on the Performance of Various Thin-Film PV Module Technologies in Tropical Singapore. IEEE J. Photovoltaics 4, 1268–1274. https://doi.org/10.1109/JPHOTOV.2014.2328585